AD-A079 984 GTE SYLVANIA INC MOUNTAIN VIEW CALIF ELECTRO-OPTICS --ETC F/G 20/3
SIMULTANEOUS SRS AND SHG IN LITHIUM IODATE. (U)
JUL 79 E O AMMANN

UNCLASSIFIED F49620-78-C-0077

AFOSR-TR-79-1328 NL

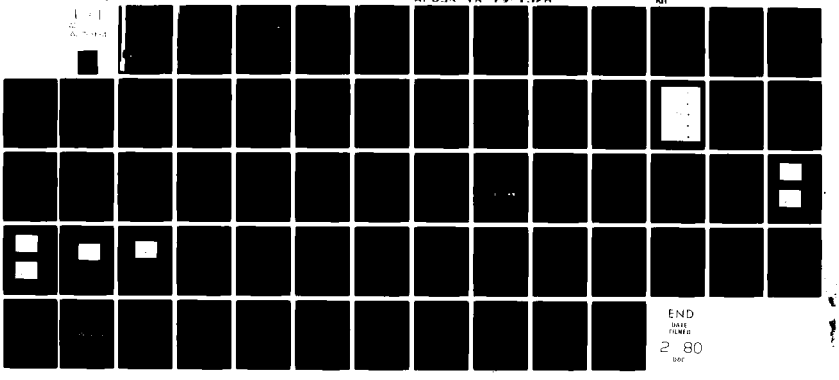

END
DATE FILMED
2 80
DDC

SIMULTANEOUS SRS AND SHG IN LITHIUM IODATE

GTE Sylvania, Inc.
Electro-Optics Organization
Mountain View, California 94042

Final Report for Period May 1978 - May 1979

July 1979

AIR FORCE OFFICE OF SCIENTIFIC RESEARCH
Bolling Air Force Base, D. C. 20332

SIMULTANEOUS SRS AND SHG IN LITHIUM IODATE

GTE Sylvania, Inc.
Electro-Optics Organization
Mountain View, California 94042

Final Report for Period May 1978 - May 1979

July 1979

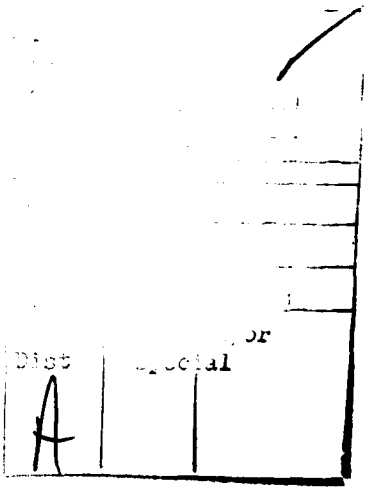

AIR FORCE OFFICE OF SCIENTIFIC RESEARCH
Bolling Air Force Base, D. C. 20332

UNCLASSIFIED

SECURITY CLASSIFICATION OF THIS PAGE (When Data Entered)

REPORT DOCUMENTATION PAGE	READ INSTRUCTIONS BEFORE COMPLETING FORM
1. REPORT NUMBER: AFOSR TR-79-1328	2. GOVT ACCESSION NO. / 3. RECIPIENT'S CATALOG NUMBER
4. TITLE (and Subtitle): SIMULTANEOUS SRS AND SHG IN LITHIUM IODATE	5. TYPE OF REPORT & PERIOD COVERED: Final rept. May 78 – May 79
	6. PERFORMING ORG. REPORT NUMBER
7. AUTHOR(s): Eugene O. Ammann	8. CONTRACT OR GRANT NUMBER(s): F49620-78-C-0077
9. PERFORMING ORGANIZATION NAME AND ADDRESS: GTE Sylvania, Inc. Electro-Optics Organization Mountain View, California 94042	10. PROGRAM ELEMENT, PROJECT, TASK AREA & WORK UNIT NUMBERS: 61102F 2301 A1 A1
11. CONTROLLING OFFICE NAME AND ADDRESS: AFOSR/NP Bolling AFB, Bldg. 410 Wash DC 20332	12. REPORT DATE: Jul 79 / 13. NUMBER OF PAGES: 64
14. MONITORING AGENCY NAME & ADDRESS (if different from Controlling Office)	15. SECURITY CLASS. (of this report): unclassified / 15a. DECLASSIFICATION/DOWNGRADING SCHEDULE

16. DISTRIBUTION STATEMENT (of this Report)

Approved for public release;
distribution unlimited.

17. DISTRIBUTION STATEMENT (of the abstract entered in Block 20, if different from Report)

18. SUPPLEMENTARY NOTES

19. KEY WORDS (Continue on reverse side if necessary and identify by block number)

1) stimulated Raman scattering
2) second harmonic generation
3) sum frequency generation
4) lithium iodate
5) multi-wavelength source

20. ABSTRACT (Continue on reverse side if necessary and identify by block number)

This report summarizes the results of ~~a twelve-month program whose goal was to~~ study the simultaneous occurrence of stimulated Raman scattering (SRS), second-harmonic generation (SHG), and sum-frequency generation (SFG) in lithium iodate. The simultaneous occurrence of these processes in lithium iodate results in selectable, multiple outputs spanning the 0.54-μm to 0.65-μm region of the visible spectrum. The SRS/SHG/SFG device consists of a lithium

next page

DD FORM 1 JAN 73 1473 EDITION OF 1 NOV 65 IS OBSOLETE

UNCLASSIFIED

SECURITY CLASSIFICATION OF THIS PAGE (When Data Entered)

406 496

JOB

20. (cont.)

iodate crystal placed inside a cw-pumped, repetitively Q-switched Nd:$YAlO_3$ laser. Two-mirror and three-mirror versions of the SRS/SHG/SFG device were studied. The two-mirror SRS/SHG/SFG average power outputs that were achieved were 0.54 μm (1.13 W), 0.565 μm (78 mW), 0.592 μm (685 mW), 0.622 μm (98 mW), and 0.655 μm (107 mW). The three-mirror SRS/SHG/SFG outputs were 0.54 μm (950 mW), 0.565 μm (218 mW), 0.592 μm (202 mW), 0.622 μm (29 mW), and 0.655 μm (26 mW). Pulses obtained from the two-mirror setup were approximately 25 to 40 ns long; pulses obtained from the three-mirror setup were 4 to 10 ns long. Experimental and analytical studies were also carried out concerning interactions which occur between the simultaneous SRS, SHG, and SFG processes.

FORWARD

This final report summarizes the twelve months of work performed on Air Force Contract F49620-78-C-0077 entitled "Simultaneous SRS and SHG in Lithium Iodate." The research described in this report was performed from May 1978 through May 1979. This report was prepared by the Electro-Optics Organization of GTE Sylvania Inc., Electronic Systems Groups - Western Division, Mountain View, California, and describes work performed in the Research and Development Department headed by Dr. T. S. Fahlen. Dr. E. O. Ammann was the principal technical investigator on this program; technical assistance was provided by S. E. Hall and C. L. Goodwin.

The work performed under this contract is administered by the Air Force Office of Scientific Research, Bolling Air Force Base, D.C. 20332. Dr. Howard Schlossberg is the technical representative for the Air Force. This report was submitted by the author in July 1979.

TABLE OF CONTENTS

LIST OF ILLUSTRATIONS

LIST OF ILLUSTRATIONS (Continued)

LIST OF TABLES

Section I

INTRODUCTION

On this program, we have studied a device which utilizes the simultaneous occurrence of stimulated Raman scattering (SRS), second-harmonic generation (SHG), and sum-frequency generation (SFG) in a single crystal to produce selectable, multiple, visible outputs. This device, originated at GTE Sylvania, has the general form shown in Figure 1. The device operates in the following manner.

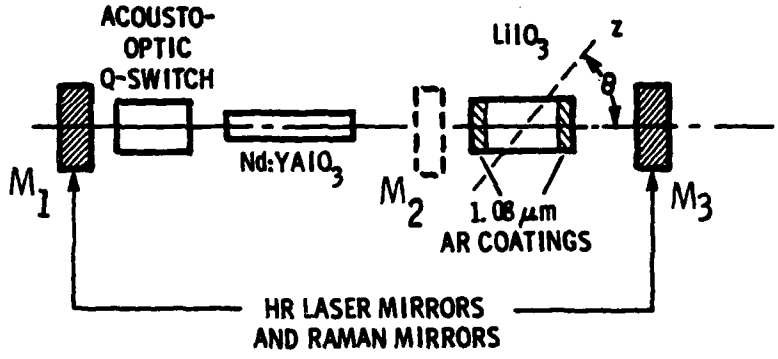

Figure 1. Basic form of SRS/SHG/SFG device

The Nd:$YA\ell O_3$ laser is continuously pumped and repetitively Q-switched, thereby producing a train of 1.08-μm pulses. Mirrors M_1 and M_3 form the resonator for this laser. This device becomes a Raman laser through the insertion of a lithium iodate ($LiIO_3$) crystal inside the laser cavity. The Stokes waves generated from this device are also resonated to provide a low threshold for the SRS. Two methods have been used to provide the Stokes resonator. The first method, a three-mirror configuration, uses mirrors M_2 and M_3 to form the Stokes resonator. In the second method, a two-mirror Raman configuration, mirror M_2 is removed and mirrors M_1 and M_3 form the Stokes resonator and the laser resonator. Both of these configurations have been investigated on this program.

The final step is that the same $LiIO_3$ crystal that is the Raman medium can also serve as a nonlinear medium and can efficiently generate phase-matched second harmonics and sum frequencies of the pump and Stokes lines. These second harmonics and sum frequencies form the useful outputs of the device. By rotating the $LiIO_3$ crystal to different phase-matching angles, one can sequentially select different SH and SF outputs. For 1.08-μm pumping of the 818 cm^{-1} vibrational mode of $LiIO_3$, we have successively generated phase-matched SH outputs at 0.54 μm, 0.592 μm, and 0.655 μm, and have generated phase-matched SF outputs at 0.565 μm and 0.622 μm.

The SRS/SHG/SFG technique that was studied on this program has gradually evolved from research that has been carried out at GTE Sylvania during the past several years. Under WPAFB sponsorship[1] in 1973, we studied optial parametric oscillation in the 1.4 to 5.1-μm region in $LiIO_3$. The pump for this optical parametric oscillator was the 1.08-μm output of a CW-pumped, repetitively Q-switched Nd:$YAlO_3$ laser operating at kHz pulse repetition rates (PRF's). During the last 2 months of that program, we discovered that SRS was occurring in the $LiIO_3$ crystal together with optical parametric oscillation. Under subsequent ERDA sponsorship[2,3] as well as GTE Sylvania IR&D programs, studies were performed of SRS in $LiIO_3$ at kHz PRF's. During these programs, substantial 1.18-μm and 1.31-μm Stokes output powers were obtained using three-mirror[4] and two-mirror[5] Raman configurations. The final step in this evolutionary process was our realization that the same $LiIO_3$ crystal that serves as the Raman medium can also be used to generate the second harmonics and sum frequencies of the pump and Stokes lines. Under a GTE Sylvania IR program, the first demonstration of the simultaneous occurrence of SRS, SHG, and SFG was carried out. This was followed by the awarding of an AFOSR contract, for which this is the final report.

The work statement for the AFOSR program specified that the following research would be carried out:

a. Experimentally determine the orientations and crystal lengths that are optimum for each of the SH and SF processes individually, and for the group of visible outputs as a whole.

b. Perform experimental and theoretical studies of the simultaneous occurrence of SRS and SHG in lithium iodate. Special attention will be given to how the two processes interact, and in particular to: (1) how SHG acts to

suppress the generation of higher order Stokes outputs, and (2) how SHG acts as a loss source for its driving SRS. Both the three-mirror and two-mirror Raman oscillator configurations will be used to carry out these studies.

c. Perform studies on the simultaneous occurrence of SRS and SFG in lithium iodate. The SFG process produces strong visible outputs, many of which occur at wavelengths that are not generated by SHG. Study analytically and experimentally the interactions between SRS and SFG. Investigate how SFG tends to suppress its driving SRS.

d. Investigate whether the visible second harmonics and sum frequencies pump their own SRS.

e. Investigate methods for recovering the "wrong way" second harmonics and sum frequencies that are generated.

f. Perform experiments and calculations that are aimed at establishing the power scalability of this technique. Determine the process(es) or component(s) that will act to limit the attainable output powers, and study ways of circumventing this limiting factor(s).

This report is organized in the following manner. Section II provides background information on SRS, SHG, and SFG in $LiIO_3$, and on the conditions that are necessary for their simultaneous occurrence. Section III gives the results of our SRS/SHG/SFG studies utilizing the two-mirror Raman configuration; Section IV gives SRS/SHG/SFG results that were attained using the three-mirror Raman Configuration. In Section V we discuss analytical and experimental investigations of the interactions that occur between simultaneously occurring SRS, SHG, and SFG. In Section VI, we give our observations on processes that might act to limit the power that can be achieved from an SRS/SHG/SFG device. Then we summarize our results and conclusions in Section VII and list publications emanating from this contract in Section VIII.

This Page Left Intentionally Blank

Section II

BACKGROUND

This section provides background information on the processes of Raman scattering, second-harmonic generation (SHG), and sum-frequency generation (SFG), with particular emphasis on these processes in $LiIO_3$. This section also describes how pairs of these (SRS and SHG, or SRS and SFG) can occur simultaneously in $LiIO_3$.

2.1 RAMAN SCATTERING

Stimulated Raman scattering (SRS) is one of the simultaneous processes encountered under this program. One method of characterizing the process of Raman scattering is as follows. A pump beam (typically from a laser) is incident upon the Raman medium. The pump beam decomposes into a Stokes output, which is photon-like, and a Raman output. The Raman output is closely tied to a natural vibrational mode of the Raman medium and can be either purely phonon-like, or partially phonon-like and photon-like in character.

In the decomposition process, conservation of energy must be satisfied as stated by the frequency equation

$$\omega_p = \omega_S + \omega_R, \tag{1}$$

and conservation of momentum must be satisfied as stated by the wavevector equation

$$\vec{k}_p = \vec{k}_S + \vec{k}_R \tag{2}$$

Subscripts p, S, and R refer to the pump, Stokes, and Raman waves, respectively.

The relationship between ω_R and k_R for the Raman mode in question depends on the type of crystal vibrational mode involved. The form of this dispersion characteristic is crucial for determining the exact Raman interaction that occurs.

2.1.1 LO and TO Vibrational Modes

All of our SRS work with $LiIO_3$ has involved so-called A_1 and E_1 symmetry modes. The A_1 and E_1 symmetry modes in $LiIO_3$ are both Raman and infrared active. The frequency of a phonon that is infrared active is split into rather closely spaced longitudinal-optic (LO) and transverse-optic (TO) components. The LO modes are phonon-like in character and have their mechanical vibration direction in the same direction as their propogation direction. The dispersion characteristic for LO modes is shown in Figure 2. The Raman frequency is constant at a value of ω_{LO}, but the mode can assume any value of k. This means that phase-matching can occur both for forward Raman scattering and backward Raman scattering as shown in details (a) and (b), respectively, of Figure 2. Furthermore, the frequency of the generated Stokes wave is the same in these two cases since ω_{LO} is the same. In showing the phase-matching of Figure 2, only colinear situations are considered. Noncolinear phase-matching of these Raman processes is also possible, but was not of importance to this program.

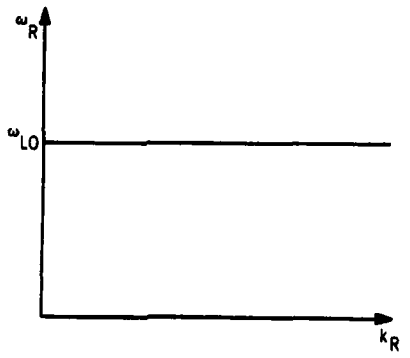

Figure 2. Dispersion curve for Raman-active and infrared-active LO vibrational mode

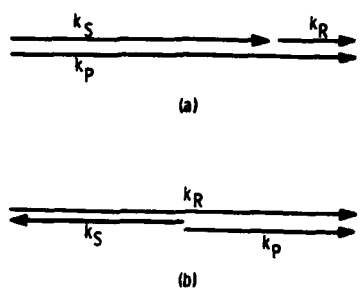

Figure 3. Colinear phase-matching for forward (a) and backward (b) Raman scattering for LO vibrational modes

The TO modes are both phonon-like and photon-like in nature, and an electromagnetic (EM) wave is associated with them. The mechanical vibration direction of TO modes is transverse to their propagation direction. Because EM waves also vibrate perpendicular to their propagation direction, TO modes exhibit strong coupling between their mechanical and EM waves. These waves are called polaritons and exhibit the dispersion characteristic shown in Figure 4. The important item to note in Figure 4 is that the polariton frequency ω_R is not constant, but rather depends strongly upon k.

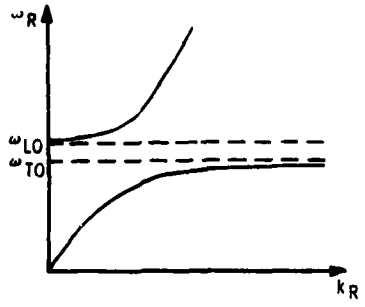

Figure 4. Dispersion curve for Raman-active and infrared-active TO vibrational modes

At least one important ramification of this dependence is that the Stokes wavelengths for forward and backward scattering will be different. Consider first

forward colinear scattering. The phase-matching situation of Figure 3(a) again applies, but now k_R is no longer free to assume any length independent of ω_R. Rather ω_R and k_R have the dependence shown in Figure 4. This dependence together with the normal $k_S = n\omega_S/c$ relationship for the EM Stokes wave must be used in order to simultaneously satisfy Equations 1 and 2. Carrying this out, point (a) is shown in Figure 5 as a typical solution for the forward-scattering case.

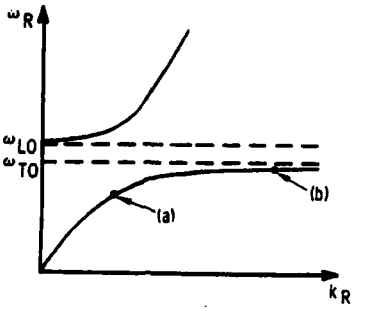

Figure 5. Typical phase-matching points for colinear phase-matching of a TO mode for (a) forward Raman scatter, and (b) backward Raman scatter

For backward scattering, the phase-matching situation of Figure 3(b) applies. In this case, a larger value of k_R is needed. A typical operating point is shown as point (b) in Figure 5. Now, we are on a more horizontal portion of the dispersion curve, and the general situation is more similar to that described for LO vibrational modes.

2.1.2 Oblique Phonons

When propagation occurs along one of the crystal axes, the symmetry properties and the Raman frequencies of the crystal modes are well known and easy to calculate. Preceding discussions in this section pertain to modes generated from such on-axis beams. However, when beam propagation is not along a crystal axis but at an angle to the axes, the resulting mode frequency and polarization changes, and the resulting mode is essentially a linear combination of the on-axis modes. Such modes are called oblique phonons and seem to occur only with modes that are both Raman and infrared active.

When the modes involved are LO modes, the dispersion curve of Figure 2 is still applicable, but ω_R is shifted to a new value. When TO modes are involved, Figure 4 still applies, but ω_{LO} and ω_{TO} are shifted to new values. Thus, oblique phonons offer the opportunity to tailor the Raman frequency somewhat by selecting the crystal orientation (or equivalently, beam-propagation direction) to be employed.

Otaguro, et al.,[6-9] have performed extensive investigations of oblique phonons in $LiIO_3$ employing spontaneous Raman scattering. Their results that are of greatest importance for the proposed program are probably best summarized in Figures 6 and 7, both adapted from Reference 7.

Figure 6 shows that the Raman frequency of $LiIO_3$ varies continuously as the crystal orientation is changed from θ = 0 to 90 degrees, where θ is the angle between the crystal optic axis and the pump beam propagation direction. The upper curve of Figure 6 varies from 817 cm^{-1} to 848 cm^{-1}, while the lower curve varies from 769 cm^{-1} to 795 cm^{-1}.

Figure 7 shows the comparative intensities of the two oblique phonon curves of Figure 6. For values of θ less than about 36 degrees, the 817 to 848 cm^{-1} branch has greater intensity and should predominate over the 769 to 795 cm^{-1} branch. Our SRS results in $LiIO_3$ have confirmed this since, for θ = 20 degrees and for θ = 26.5 degrees we have always obtained SRS on the upper branch.

2.1.3 Generation of Second Stokes Outputs

Section 2.1.1 described how a pump photon can decompose into a Stokes photon and a Raman phonon. It is also possible for this process to repeat itself, with the first Stokes wave now acting as the pump and decomposing into a second Stokes photon and a Raman phonon. Equations that are similar to Equations 1 and 2 can be written giving

$$\omega_{S1} = \omega_{S2} + \omega_R \tag{3}$$

and

$$\vec{k}_{S1} = \vec{k}_{S2} + \vec{k}_R, \tag{4}$$

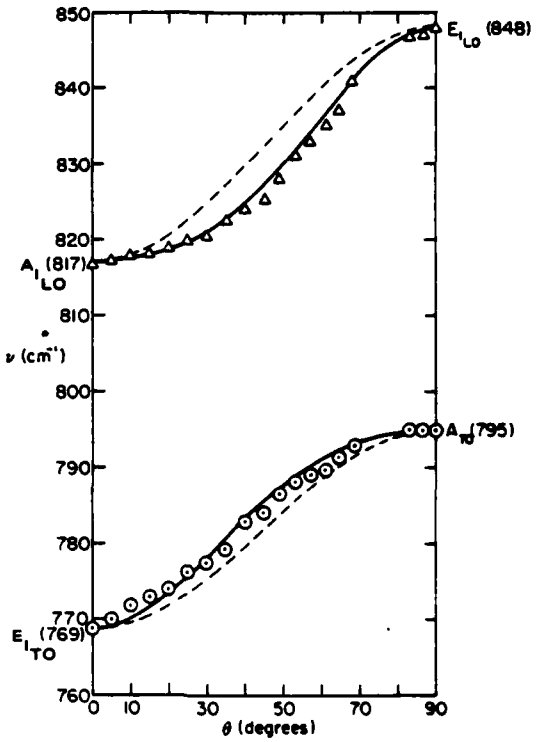

Figure 6. Angular dispersion of the A_1 and E_1 symmetry oblique phonons propagating in the XZ (or equivalently, the YZ) plane of $LiIO_3$

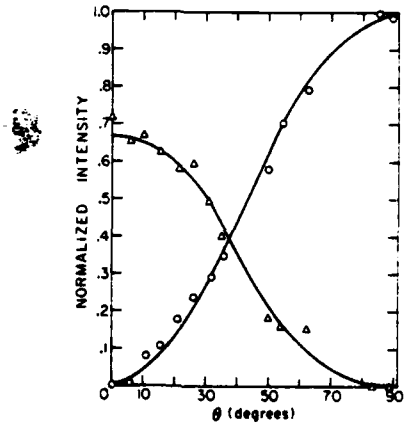

Figure 7. Raman normalized Intensities of oblique phonons (intensities have been normalized to the intensity of A_{TO} = 795 cm^{-1} at $\theta = 90^{o}$)

where the subscripts S1 and S2 denote first Stokes and second Stokes, respectively. Note that the subscript S used in Equations 1 and 2 could now be changed to S1 to emphasize that we are dealing with the first Stokes wave in that discussion.

It is possible for the Raman process to continue even further, with a second Stokes photon decomposing into a third Stokes photon and a Raman phonon. In general, the process gradually becomes weaker as we continue to higher orders.

2.2 SECOND-HARMONIC GENERATION AND SUM-FREQUENCY GENERATION

The other processes that are of importance on the proposed program are SHG and SFG. We may view SHG in the following simplified manner. Two photons at the fundamental (pumping) wavelength merge to produce a single photon at the second-harmonic wavelength.

In this process, conservation of energy is again required, giving

$$2\omega_F = \omega_{SH} \tag{5}$$

and conservation of momentum similarly requires that

$$2k_F = k_{SH}. \tag{6}$$

In Equations 5 and 6, subscripts F and SH refer to the fundamental and second harmonic, respectively. To achieve the phase-matching condition implicit in Equation 6, SHG in $LiIO_3$ utilizes an O-ray as the fundamental and generates a second harmonic polarized as an E-ray (Type I phase-matching). In addition, the $LiIO_3$ crystal must be oriented at the correct phase-matching angle, θ, to satisfy Equation 6.

The process of sum-frequency generation (SFG) is very similar to that of SHG. In SFG, two photons having different frequencies mix together to generate their sum frequency. Once again, conservation of energy and conservation of momentum must be satisfied, giving

$$\omega_{F1} + \omega_{F2} = \omega_{SF} \tag{7}$$

and

$$\vec{k}_{F1} + \vec{k}_{F2} = \vec{k}_{SF} \tag{8}$$

where F1 and F2 are the dissimilar driving frequencies and SF is the resulting sum frequency. The two driving frequencies are O-rays in $LiIO_3$ and the resulting sum frequency in an E-ray.

2.3 SATISFACTION OF PHASE-MATCHING CONDITIONS FOR SIMULTANEOUS SRS AND SHG IN $LiIO_3$

Thus far, we have shown how $LiIO_3$ can produce SRS. But if the $LiIO_3$ crystal orientation has been properly chosen and if the various spectral components are properly polarized, phase-matched generation of the second harmonics or the sum frequencies of the pump and Stokes waves will occur. This subsection shows how the conditions needed for obtaining both SRS and SHG or SRS and SFG can be simultaneously satisfied in a single $LiIO_3$ crystal.

We first note that the various spectral components involved have the correct linear polarizations to allow simultaneous SRS and SHG to occur. GTE Sylvania SRS work to date [2-5] has shown that SRS is strongest in $LiIO_3$ when the pumping beam is polarized as an ordinary ray. All Stokes beams generated from this SRS are also ordinary rays. The SHG (and SFG) processes in $LiIO_3$ must utilize Type I phase-matching for which the two fundamental photons that generate the SH (or SF) photon need to be similarly polarized. For $LiIO_3$, the required polarization of the fundamental beam is an ordinary ray and the resulting generated SH (SF) is an extraordinary ray. Thus we see that the Stokes beams from the device shown in Figure 1 are indeed correctly polarized to pump the SH and SF processes that are of interest for the proposed program.

Another consideration is whether phase-matching can be achieved for the simultaneous occurrence of SRS and SHG. On all of our previous SRS work in $LiIO_3$ [2-5], SRS has occurred on the (817) to (848) LO oblique phonon branch of Figure 6. For purposes of this example, we will assume that this continues to be the case. By using the data of Figure 6, we can plot the expected Stokes wavelengths as a function of θ, the $LiIO_3$ crystal orientation. The resulting curves are shown in Figure 8. Because the Raman frequency varies a relatively small amount in Figure 6 versus θ, we would expect the changes in the Stokes wavelengths to also be

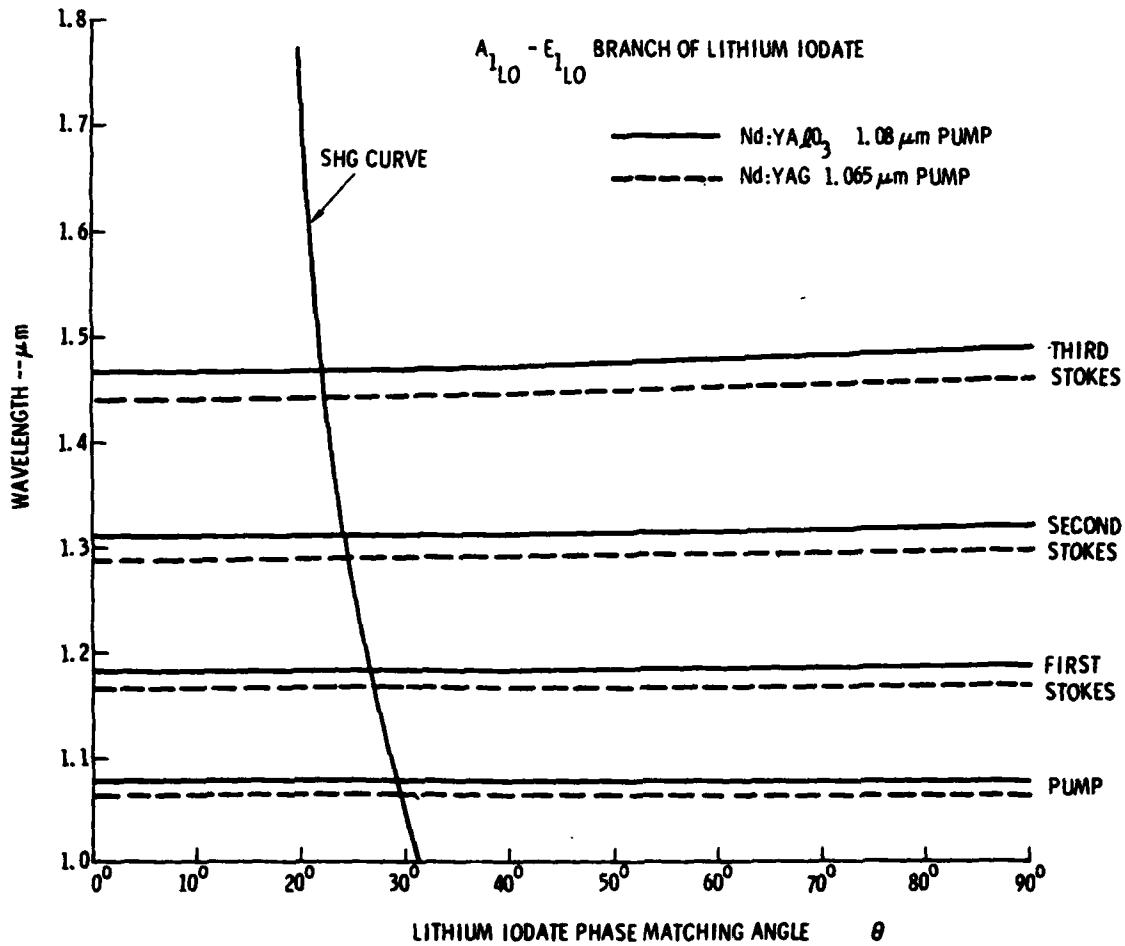

Figure 8. SRS and SHG phase-matching curves for the (817)-(848)cm^{-1} LO mode of $LiIO_3$

relatively small. We find that this is indeed the situation. If one chooses to pump the Raman oscillator with Nd:YAG instead of Nd:YAℓO_3, similar Stokes wavelength curves result and these are shown by the dashed lines in Figure 8.

In reference to the SHG phase-matching curve for $LiIO_3$, using published data on the indices of refraction of $LiIO_3$, we could easily calculate values of the fundamental wavelength that will produce phase-matched SHG versus θ. Instead we will use

an experimental SHG curve by Campillo[10]. The curve is plotted in Figure 8. We see that this SHG curve does indeed intersect each of the Stokes wavelength curves, thereby confirming that simultaneous SRS and SHG can occur. In a similar fashion, we could also have plotted an SFG curve in Figure 8 that intersects the Stokes wavelength curves.

It can be noted from Figure 8 that the required crystal orientation will be somewhat different for phase-matching each of the SFG or SHG processes. If we assume that a Nd:$YA\ell O_3$ pump laser is used, crystal angles of 26.5 degrees, 24 degrees, and 22 degrees will be needed to generate the second harmonics of the first, second, and third Stokes beams, respectively. If we choose to generate the second harmonic of the 1.08μm pump, a crystal angle of 29 degrees will be needed. If we choose to generate the sum frequency of the pump and first Stokes beams, a crystal angle of about 28 degrees will be needed; and if we generate the sum frequency of the first and second Stokes beams, a crystal angle of about 25.5 degrees is required. Because the required crystal angles are different for phase-matching each process, we are able to choose a crystal orientation that will efficiently produce only one SH or SF (i.e., we are able to get a single color out of our laser). On the other hand, the range of crystal angles is small enough that crystal rotation can be used to produce (stepwise) tunability of the visible outputs. The five sum frequencies and second harmonics we have obtained by pumping $LiIO_3$ with 1.08μm are shown in Figure 9.

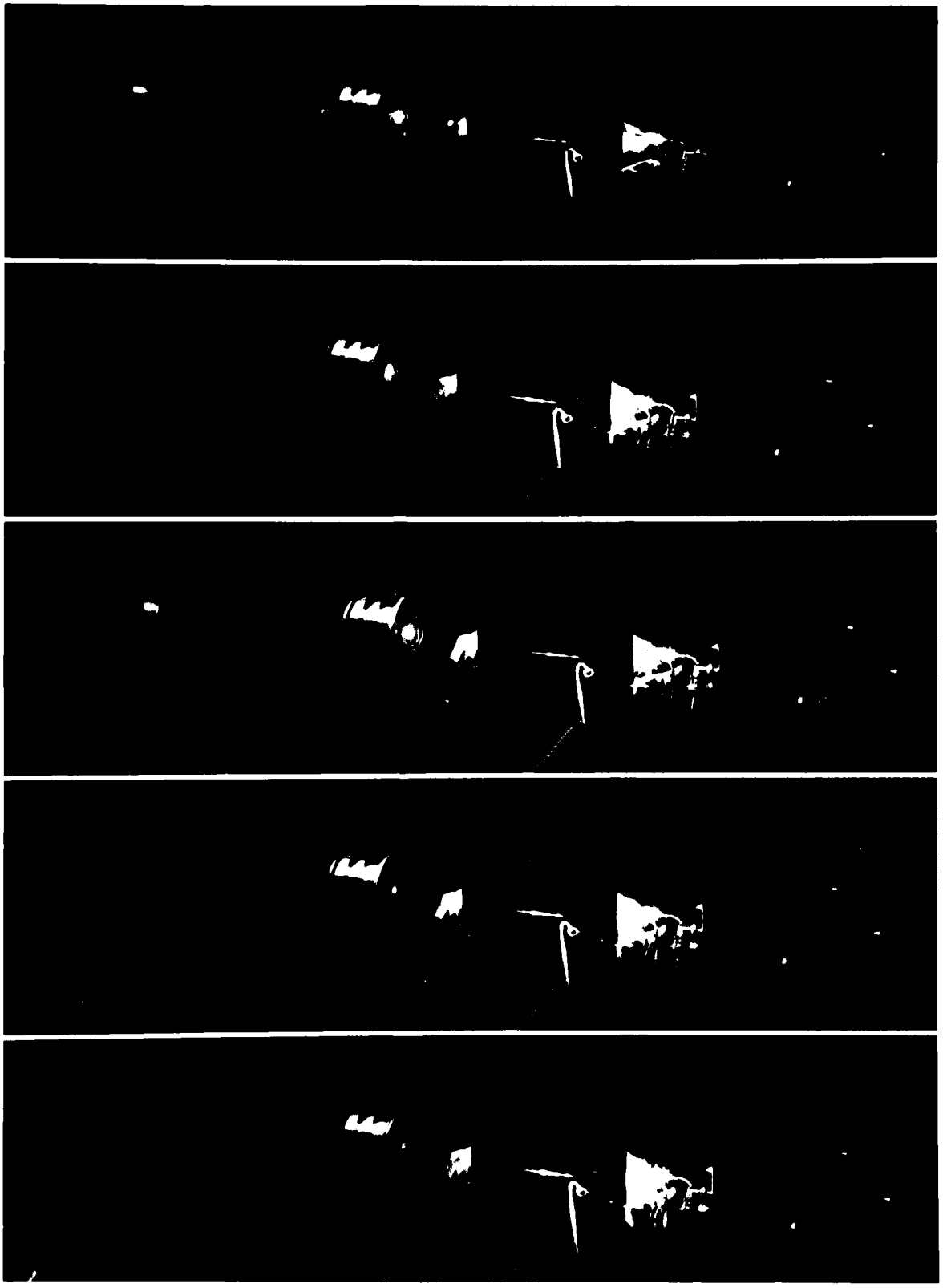

Figure 9. Visible outputs obtained from 1.08μm pumped $LiIO_3$ SRS/SHG/SFG device

Section III

TWO-MIRROR SRS/SHG/SFG EXPERIMENTAL RESULTS

On this program, SRS/SHG/SFG experiments have been carried out using the two-mirror Raman configuration of Figure 10. Some of these experiments were carried out using a 4-centimeter long $LiIO_3$ crystal while others were carried out using a 6-centimeter long $LiIO_3$ crystal. In addition, some experiments recovered only one of the two oppositely generated SH and SF outputs, while others recovered both beams. In this section, we describe the results of all two-mirror SRS/SHG/SFG experiments that were performed on this program. These two-mirror SRS/SHG/SFG results are also summarized in Reference 11.

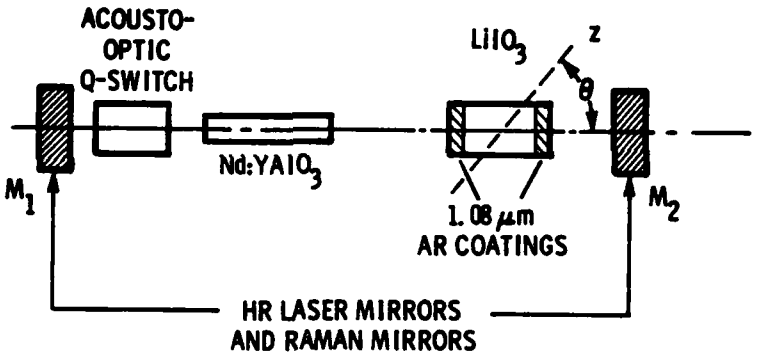

Figure 10. Configuration of two-mirror SRS/SHG/SFG device

3.1 RESULTS OBTAINED USING 4-CENTIMETER $LiIO_3$ CRYSTAL

We begin by reviewing the results achieved when a 4-centimeter-long $LiIO_3$ crystal having $\theta = 26.5$ degrees was employed. Measurements were made of the power outputs in each of the SH and SF visible lines. In all cases concerning the 4-centimeter-long crystal, the SH and SF outputs represent "one-way" powers that are generated in a single direction in the $LiIO_3$ and transmitted through mirror M_2.

Equal visible powers were also generated in the opposite direction in the $LiIO_3$ but were not recovered in these experiments. Second-harmonic output powers at 0.592 and 0.655μm were measured versus PRF and the results are shown in Figures 11 and 12. In each figure, the available 1.08μm pump powers are also shown, together with the pertinent Stokes powers. To measure the available 1.08μm powers, mirror M_2 was replaced by a mirror having 4 percent transmission at 1.08μm. The first and second Stokes powers of Figure 11 and 12 were measured by replacing mirror M_2 with mirrors that were 13 percent transmitting at 1.18μm and 14 percent transmitting at 1.31μm, respectively. All measurements were taken with an electrical power of approximately 3 kilowatts into the laser lamps.

From Figure 11 we see that sizable outputs were obtained from the SH of the first Stokes line at 0.592μm. The data of Figure 11 help to emphasize that both the SRS and SHG processes are quite efficient in $LiIO_3$. Conversion efficiencies from pump to first Stokes power can be in the 40- to 50-percent range. Then, if one considers "two-way" SH power instead of one-way, the resulting SH power can be essentially as great as the first Stokes power. After the power-versus-PRF data of Figure 11 had been taken, the PRF was set at 4 kHz and all components carefully adjusted to produce maximum 0.592μm output. We obtained our best, one-way, 0.592μm power of 685 milliwatts from this experiment, with corresponding 1.18μm and 1.08μm powers of 1.27 watts and 3.1 watts, respectively.

Output powers obtained for the SH of the second Stokes are shown in Figure 12. A maximum value of 107 milliwatts of one-way, 0.655μm average powers was obtained at a 3 kHz PRF. The available 1.31μm and 1.08μm powers were 383 milliwatts and 1.4 watts, respectively.

Conventional internal SHG of the pump was also carried out with the results listed in Table I. During 0.540μm SHG, Raman processes do not enter in at all, and in fact, are suppressed by the occurrence of the SHG. The 0.540μm results serve primarily as a reference with which other SHG and SFG results can be compared.

For the 0.565μm and 0.622μm sum frequencies, power measurements were carried out only at a 3 kHz PRF. The results are given in Table I together with a summary of our 3 kHz SHG results. The average powers of 78 milliwatts and 98 milliwatts are generally lower than those attained in SHG, partially because of the occurrence of

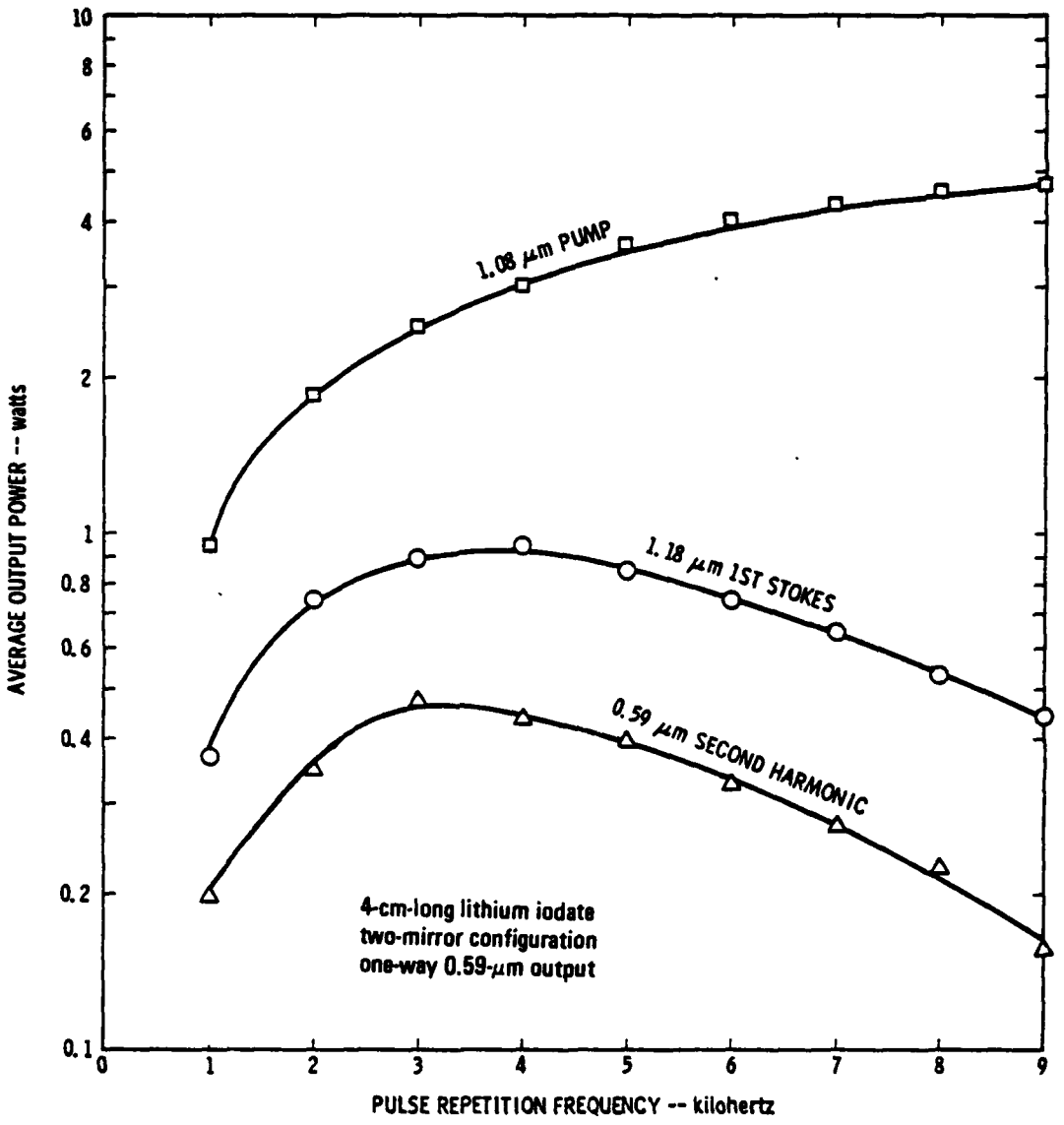

Figure 11. Pump, first-Stokes, and (one-way) 0.592μm SH average powers obtained from two-mirror Raman configuration using 4 centimeter long $LiIO_3$ crystal.

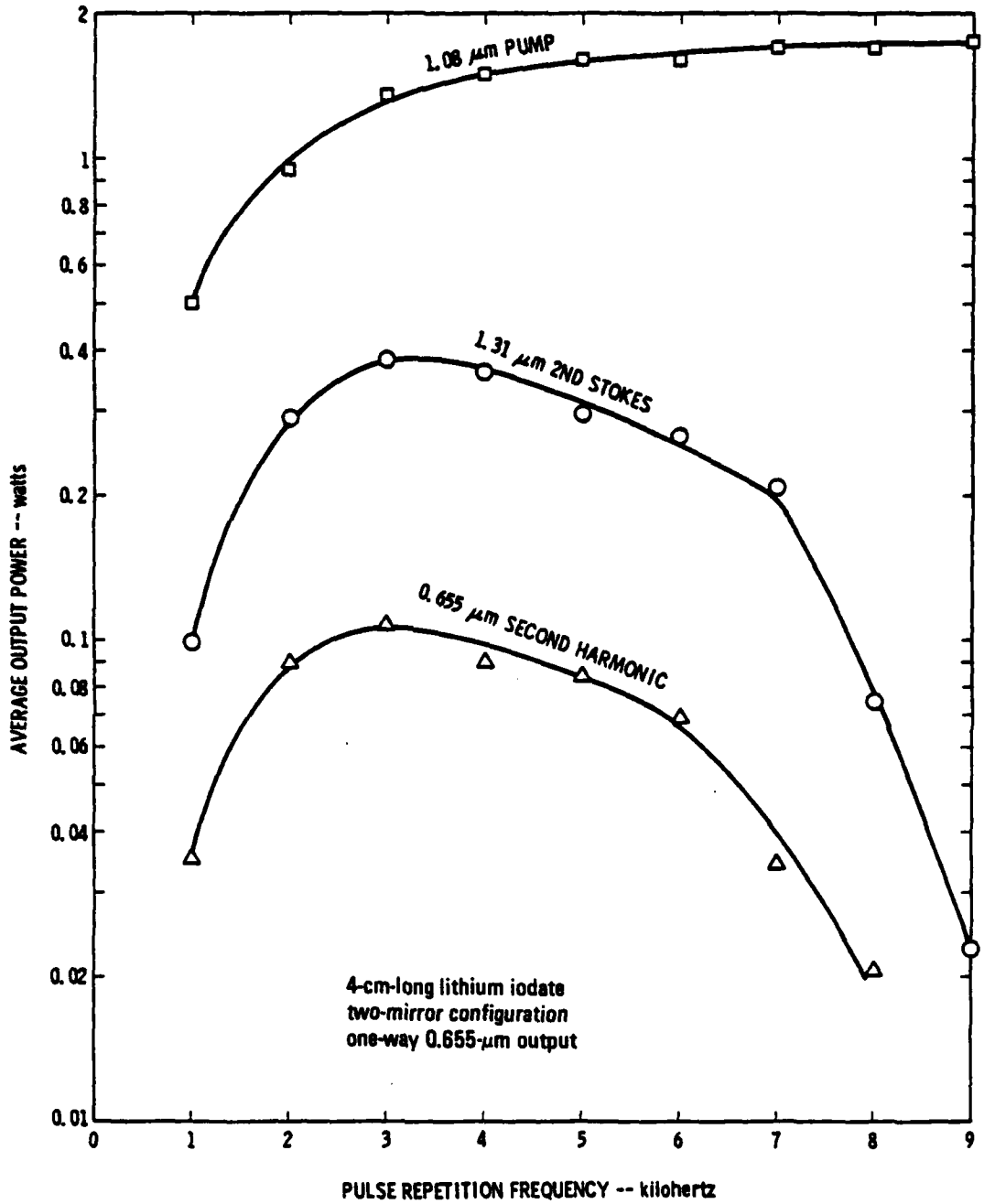

Figure 12. Pump, second-Stokes, and (one-way) 0.655μm SH average powers obtained from two-mirror Raman configuration using 4 centimeter long $LiIO_3$ crystal.

an interesting phenomenon. Namely, the occurrence of SFG tends to rather efficiently suppress the longer of the two wavelengths that are driving it. That is, 0.565μm SFG tends to extinguish the 1.18μm first Stokes while 0.622μm SFG tends to extinguish the 1.31μm second Stokes. The sum-frequency powers listed in Table I were obtained by rotating the $LiIO_3$ crystal slightly away from perfect SFG phase-matching, thereby reducing the suppression effect. This effect and other interesting interactions between the SRS and nonlinear processes are discussed in greater detail in Section 5 of this proposal.

Table I. Summary of SRS/SHG/SFG experimental results obtained at a 3 kHz PRF using a 4 centimeter long $LiIO_3$ crystal in a two-mirror Raman resonator

OUTPUT WAVE-LENGTH	NON-LINEAR PROCESS	DRIVING BEAM (S)	MEASURED PHASE MATCHING ANGLE θ	PRF	AVERAGE ONE-WAY OUTPUT POWER	PULSE LENGTH	PEAK PULSE POWER
0.540 μm	SHG	PUMP	29.4°	3 kHz	1.13 W	160 ns	2.35 kW
0.565 μm	SFG	PUMP AND FIRST STOKES	28.0°	3 kHz	78 mW	40 ns	.65 kW
0.592 μm	SHG	FIRST STOKES	26.7°	3 kHz	472 mW	45 ns	3.50 kW
0.622 μm	SFG	FIRST STOKES AND SECOND STOKES	25.4°	3 kHz	98 mW	30 ns	1.08 kW
0.655 μm	SHG	SECOND STOKES	24.2°	3 kHz	107 mW	25 ns	1.43 kW
1.080 μm				3 kHz	2.0 W	140 ns	4.75 kW

3.2 RESULTS OBTAINED USING 6-CENTIMETER $LiIO_3$ CRYSTAL

It is important to know whether SRS/SHG/SFG device performance can be improved through the use of longer $LiIO_3$ crystals. To answer this question, a limited number of experiments were performed using a 6-centimeter-long $LiIO_3$ crystal that was oriented with $\theta = 26.7$ degrees. This is the longest Raman crystal that we have tried in our SRS/SHG/SFG experiments.

The first experiment that utilized the 6-centimeter-long $LiIO_3$ crystal was (one-way) 0.592μm SHG. The results of this experiment are shown in Figure 13 where, once again, we show 1.08μm, 1.18μm, and 0.592μm average output powers plotted as a function of laser PRF. These results are to be compared with those of Figure 11 which are for the 4-centimeter-long $LiIO_3$ crystal. From Figure 13, we see that the

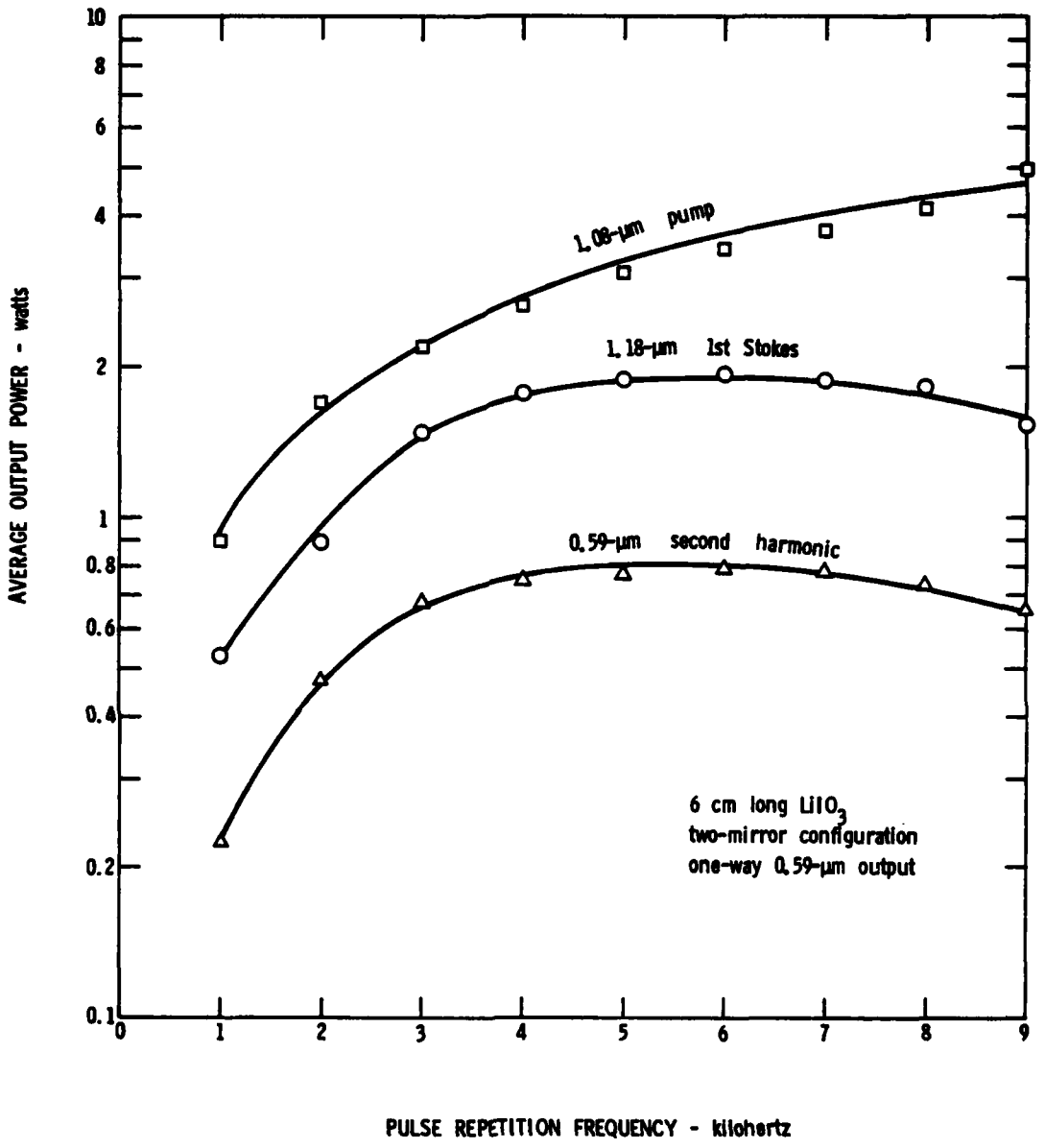

Figure 13. Pump, first-Stokes, and (one-way) 0.592μm SH average powers obtained from two-mirror Raman configuration using 6 centimeter $LiIO_3$ crystal.

attainable 1.18μm output powers were some 50 percent larger for the 6-centimeter-long crystal than for the 4-centimeter-long crystal. The 1.9 watts of 1.18μm power that was obtained at a 6 kHz PRF represents the largest first-Stokes average power yet attained. Our first conclusion, then, is that SRS is stronger for the greater $LiIO_3$ crystal length.

Referring to the 0.592μm curve of Figure 13, we have increased our 0.592μm one-way output to 791 milliwatts, compared to the 685 milliwatts we had obtained previously. This increase is more modest than the first-Stokes increase, but this is not unexpected because beam walkoff, due to double-refraction, limits the SHG efficiencies for very long crystals. Note that this limitation does not occur for the SRS where all beams are ordinary rays.

Another experiment was performed with the 6-centimeter-long crystal in which 1.31μm second-Stokes output powers were measured. The results are given in Figure 14; these results are to be compared to those of Table II of Reference 5 which are for a 4-centimeter-long crystal. Once again, we see that the Stokes output shows marked improvement, being 777 milliwatts for the 6-centimeter crystal versus 550 milliwatts for the 4-centimeter crystal.

The final experiment we performed using the 6-centimeter-long crystal was 0.592μm SHG in which the "wrong-way" 0.592μm output was recovered. To recover the wrong-way SH output, we inserted the mirror M_2 as shown in Figure 1. Mirror M_2 was highly reflecting (HR) at 0.592μm and highly transmitting (HT) at 1.18μm and 1.31μm, thus maintaining the two-mirror nature of the resonator for the SRS. The results that were obtained are shown in Figure 15. We see that the two-way 0.592μm powers were greater by about about a factor of 1.8 than the corresponding one-way powers, indicating that the wrong-way SH was being efficiently recovered. The likely reason that the 0.592μm increase was less than exactly a factor of 2.0 is that mirror M_2 presented a moderate insertion loss to the $Nd:YA\ell O_3$ laser.

From these 6-centimeter-long crystal results, we can draw the two important conclusions:

(1) Long $LiIO_3$ crystals produce stronger SRS and, consequently larger Stokes and SH output powers.

(2) The insertion of the mirror M_2 is an effective technique for recovering wrong-way SH or SF outputs.

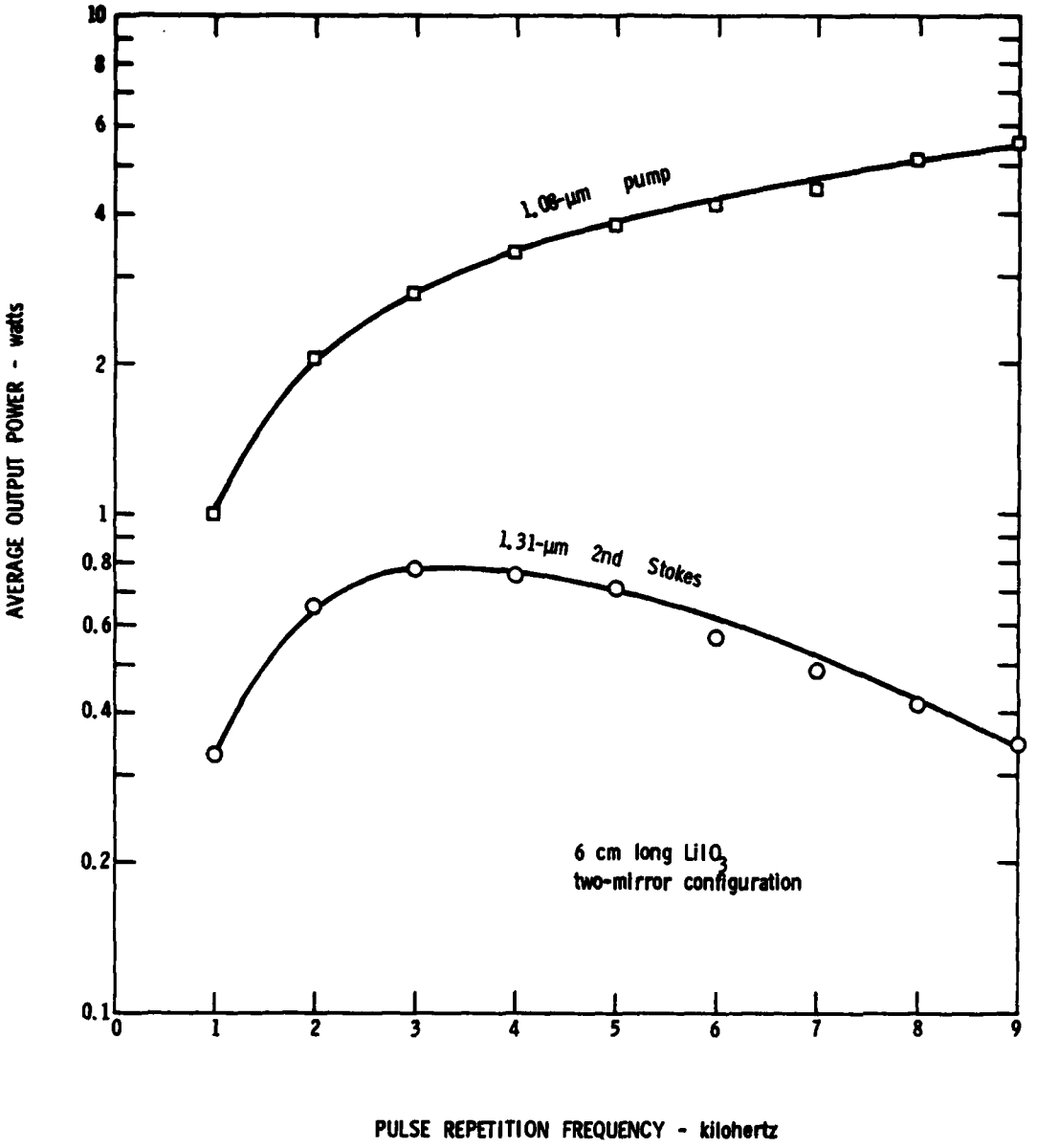

Figure 14. Pump and second-Stokes average powers obtained from two-mirror Raman configuration using 6 centimeter $LiIO_3$ crystal.

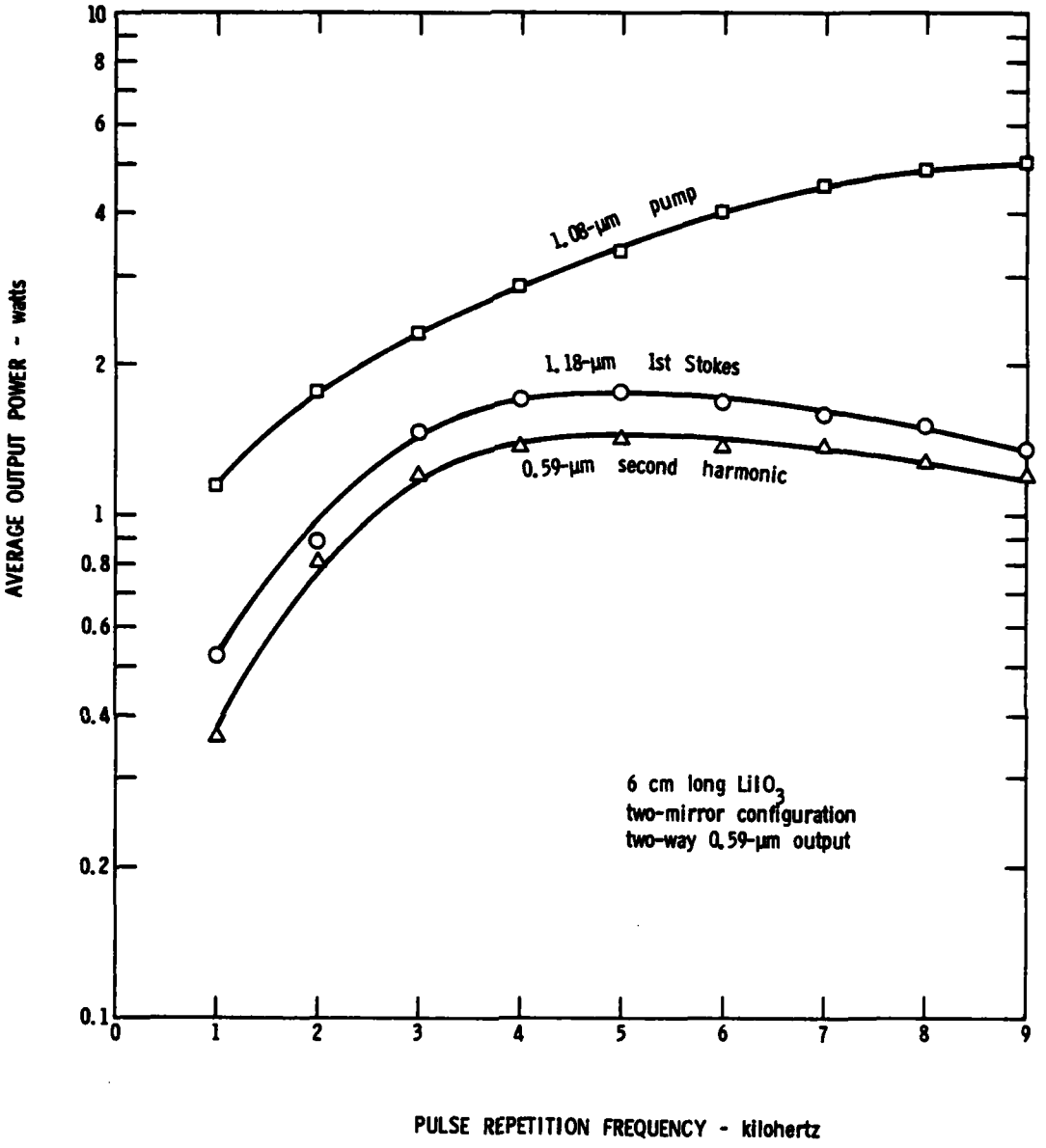

Figure 15. Pump, first-Stokes, and (two-way) 0.592μm SH average powers obtained from two-mirror Raman configuration using 6 centimeter $LiIO_3$ crystal

Both of these results have important bearing on the design of higher power versions of SRS/SHG/SFG devices.

Section IV

THREE-MIRROR SRS/SHG/SFG EXPERIMENTAL RESULTS

SRS/SHG/SFG experiments were also carried out using the three-mirror Raman configuration of Figure 16. Measurements were made of the average outputs in each of the visible second-harmonic and sum-frequency lines as a function of PRF for the three-mirror configuration. All three-mirror experiments were run using a $LiIO_3$ crystal that was 4 centimeters long and all experiments recovered only the "one-way" SH or SF. The results of these measurements are shown in Figures 17, 18, 22, 23, and 24. In these figures, the second-harmonic and sum-frequency curves represent "one-way" powers that are generated in a single direction in the $LiIO_3$ and are transmitted through Mirror M_3. Equal visible powers were also generated in the opposite direction in the $LiIO_3$ but were not recovered in our experiments.

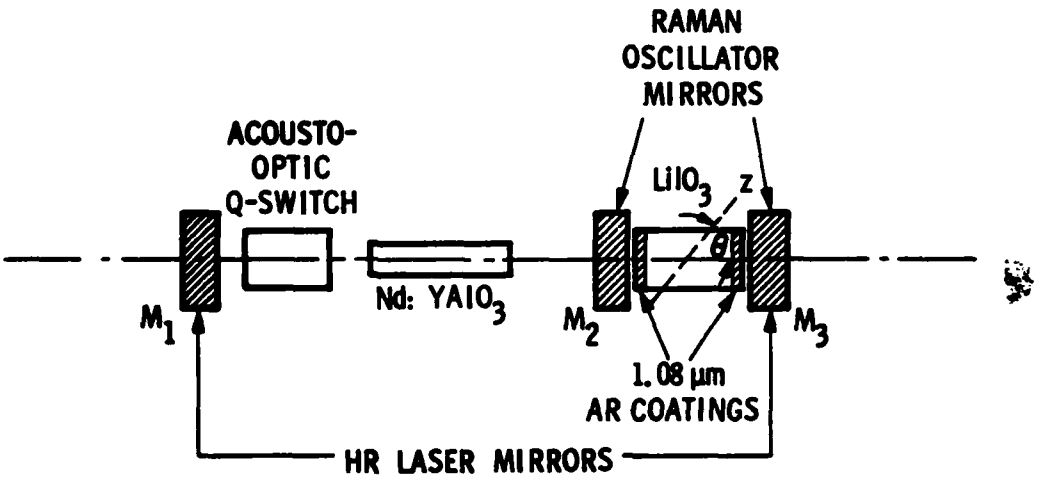

Figure 16. Configuration of three-mirror SRS/SHG/SFG device

Measurements were also taken of the pump and Stokes average powers that are available. To measure the available 1.08μm powers, mirror M_3 was replaced by a

mirror having 4-percent transmission at 1.08μm. The available first- and second-Stokes powers were measured by replacing mirror M_3 with mirrors that are 13 percent transmitting at 1.18μm and 14 percent transmitting at 1.31μm, respectively. The $LiIO_3$ crystal was also rotated slightly away from exact phase-matching during these measurements so that available Stokes powers could be measured in the absence of SHG or SFG. We noted that the mirrors used to measure available pump and Stokes powers in these experiments are the same mirrors that were used to measure available powers in the two-mirror SRS/SHG/SFG experiments.

In Figures 17, 18, 22, 23, and 24, the circles, triangles, and squares represent measured values. The solid lines in these figures are smooth curves that have been drawn through the experimental points.

The three-mirror SRS/SHG/SFG results are summarized in Reference 12.

4.1 0.592μm SECOND HARMONIC

In this experiment, the $LiIO_3$ crystal was rotated to $\theta = 26.7$ degrees, the angle at which SHG of the 1.18μm first Stokes is phase-matched. The resulting one-way 0.592μm SH outputs are plotted as a function of PRF in Figure 17. The maximum 0.592 μm average power obtained was approximately 200 milliwatts at a 2.5 kHz PRF. For comparison, the maximum 0.592μm average power obtained using the two-mirror configuration was 685 milliwatts. The smaller 0.592μm average power obtained for the three-mirror case is not unexpected, because we have previously found that Stokes average output powers are generally less from the three-mirror configuration[4] than from the two-mirror configuration[5].

The available three-mirror 1.18μm and 1.08μm average powers are also shown in Figure 17. These curves show that the SRS and SHG conversion efficiencies are substantial, particularly for PRF's in the 1 to 4 kHz range. It should also be noted, however, that the available 1.18μm first-Stokes power of Figure 17 is somewhat less than corresponding values obtained in our straight three-mirror SRS experiments[4]. This is true, in fact, for all the available Stokes powers in Figures 17, 18, 22, 23, and 24. The primary cause of this is that for each of the Stokes measurements of Figures 17, 18, 22, 23, and 24, the $LiIO_3$ crystal was tilted (nearly) to the appropriate phase-matching angle needed for SHG and SFG. In carrying out the experiments of Reference 4, however, we found that Stokes outputs were always greatest when the $LiIO_3$ was oriented with the end faces normal to the 1.08μm pump.

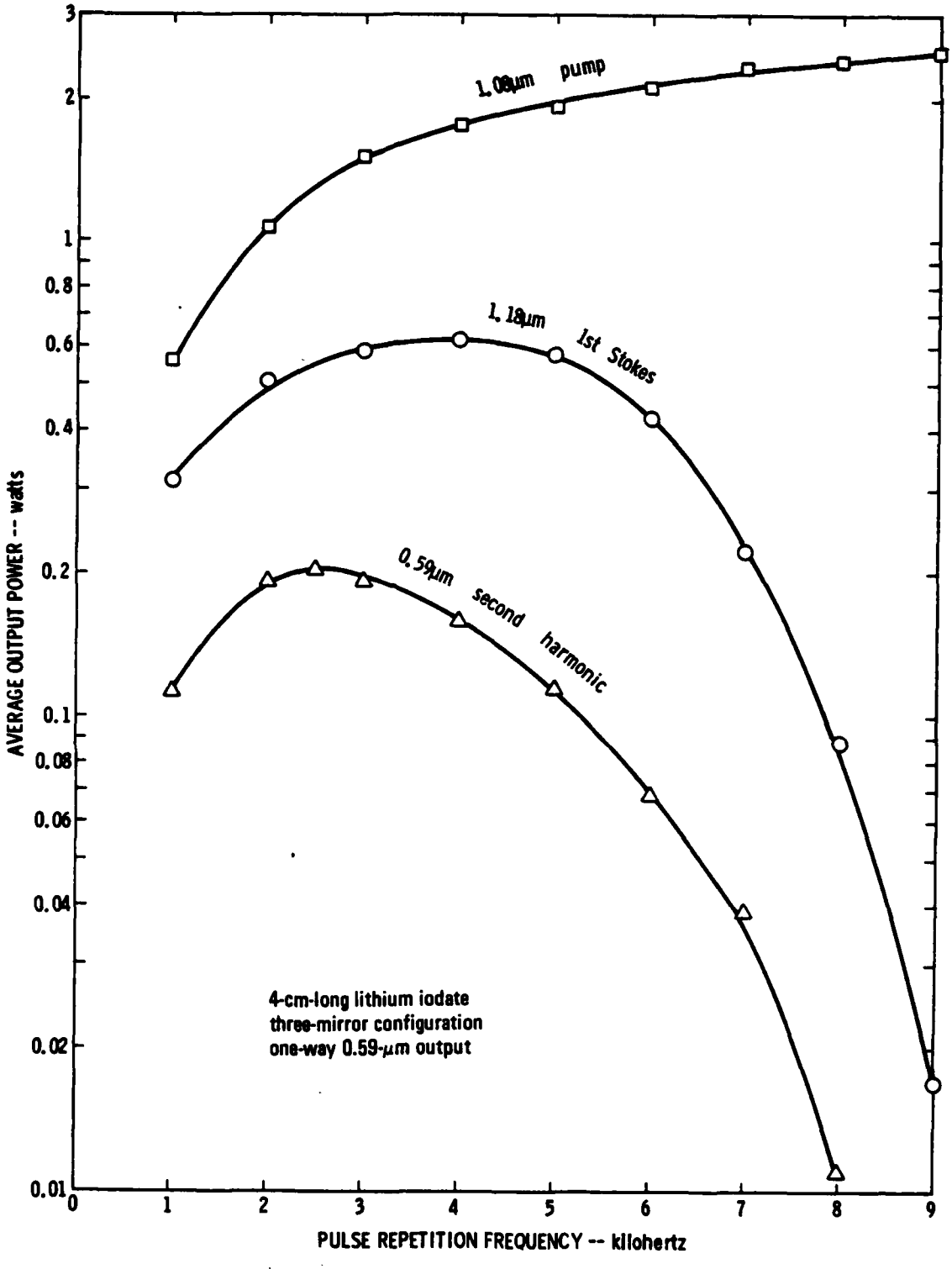

Figure 17. Pump, first-Stokes, and (one-way) 0.592μm SH average powers

Thus, all measurements in Reference 4 were taken with the $LiIO_3$ at normal incidence, while all three-mirror SRS/SHG/SFG measurements were taken at non-normal incidence.

One of the important features of the three-mirror Raman configuration is that it produces very short Stokes pulses[4]. The SH and SF pulses that are obtained from three-mirror SRS/SHG/SFG should, therefore, be correspondingly short, and this is indeed the case. The three-mirror 0.592μm pulses were found to be 11 nanoseconds long at a 3 kHz PRF, versus the 45-nanosecond pulse length found from our two-mirror experiment. The three-mirror 0.592μm pulses would be shorter yet if it were not for the occurrence of pulse-stretching during internal SHG[13,14]. During SHG, the 1.18μm pulses are some 14 nanoseconds long while, without SHG, the 1.18μm pulses are about 8 nanoseconds long. With their short duration, the 0.592μm pulses have a greater peak value for the three-mirror case than for the two-mirror case (6.1 kilowatts versus 3.8 kilowatts).

4.2 0.565μm SUM FREQUENCY

Three-mirror experiments were also carried out on the 0.565μm sum frequency generated from pump and first-Stokes beams. In these experiments, the $LiIO_3$ was rotated to its phase-matching angle of $\theta = 28.0$ degrees. The resulting one-way 0.565μm output together with available 1.18μm and 1.08μm powers are plotted in Figure 18.

Surprisingly, we obtained larger 0.565μm average powers from the three-mirror configuration than we had previously from our two-mirror experiments. The three-mirror experiment produced a 0.565μm average output of 139 milliwatts versus a best two-mirror output of 78 milliwatts.

We believe the superior three-mirror performance is due primarily to the following effect. The 1.08μm pump depletes in a significantly different manner for the three-mirror and two-mirror SRS cases[5]. Figure 19 illustrates the depletion behavior for these two cases. In the three-mirror case, some fraction (about one-third in Figure 19a of the 1.08μm pump pulse is depleted by the onset of SRS. In the two-mirror case, the 1.08μm pump pulse is depleted to virtually zero. Thus in the two-mirror case, SFG occurs utilizing a falling 1.08μm pulse and a rising 1.18μm pulse. In the three-mirror case, however, the 1.08μm pulse is only partially depleted leaving ample 1.08μm energy to mix with the 1.18μm pulse.

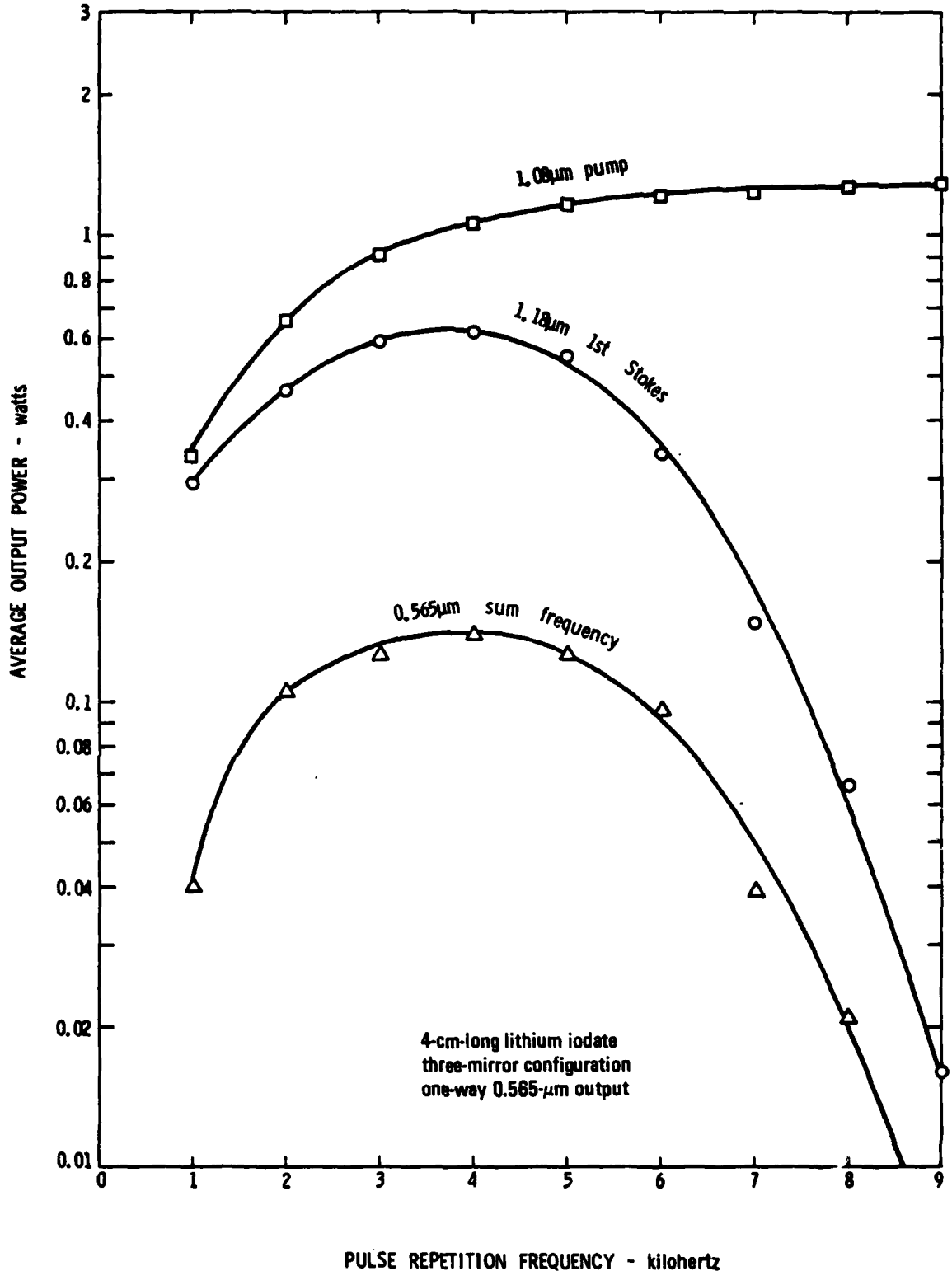

Figure 18. Pump, first-Stokes, and (one-way) 0.565μm SF average powers

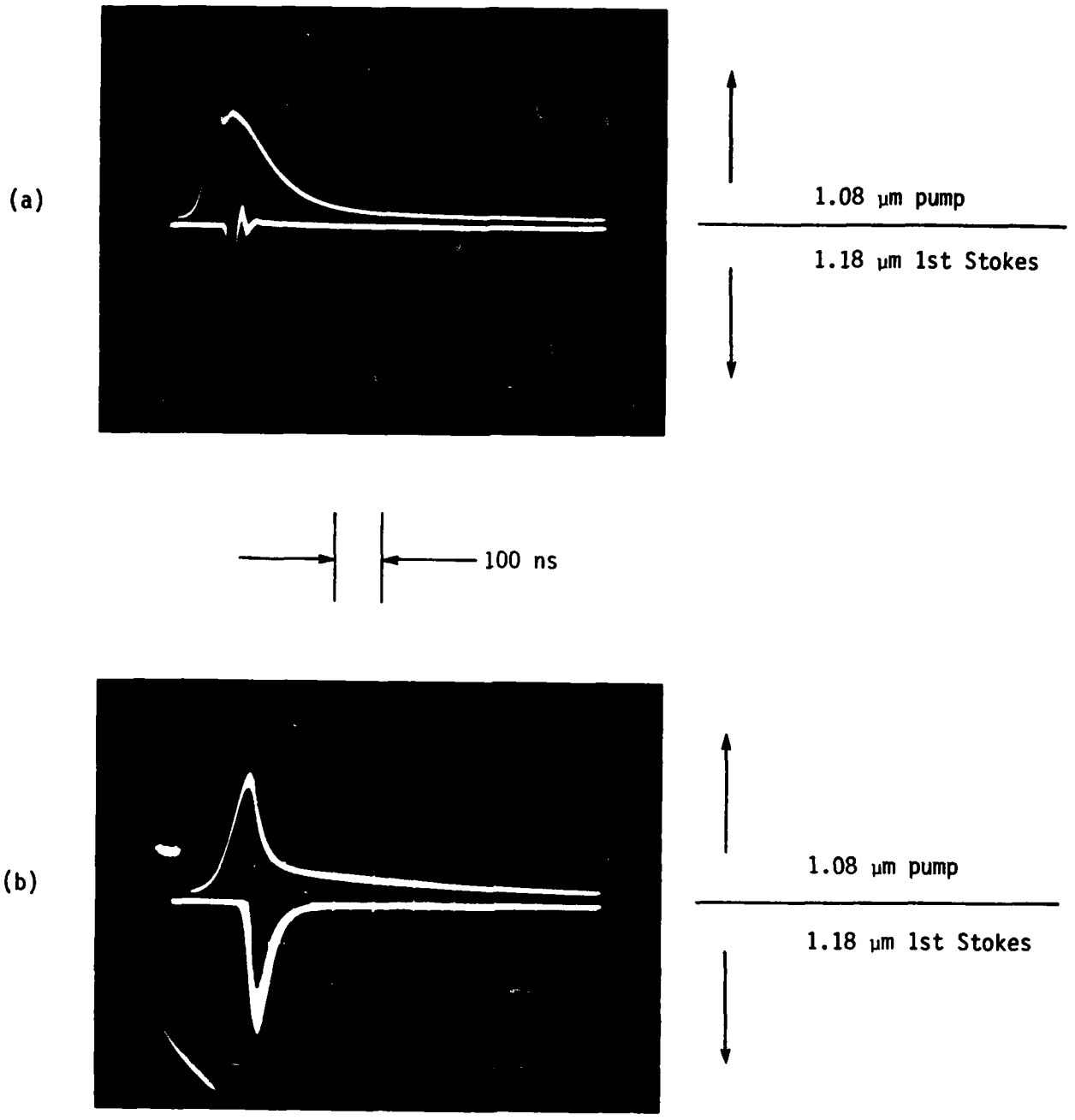

Figure 19. Pump Pulse Depletion for SRS in (a) Three-Mirror Configuration and (b) Two-Mirror Configuration

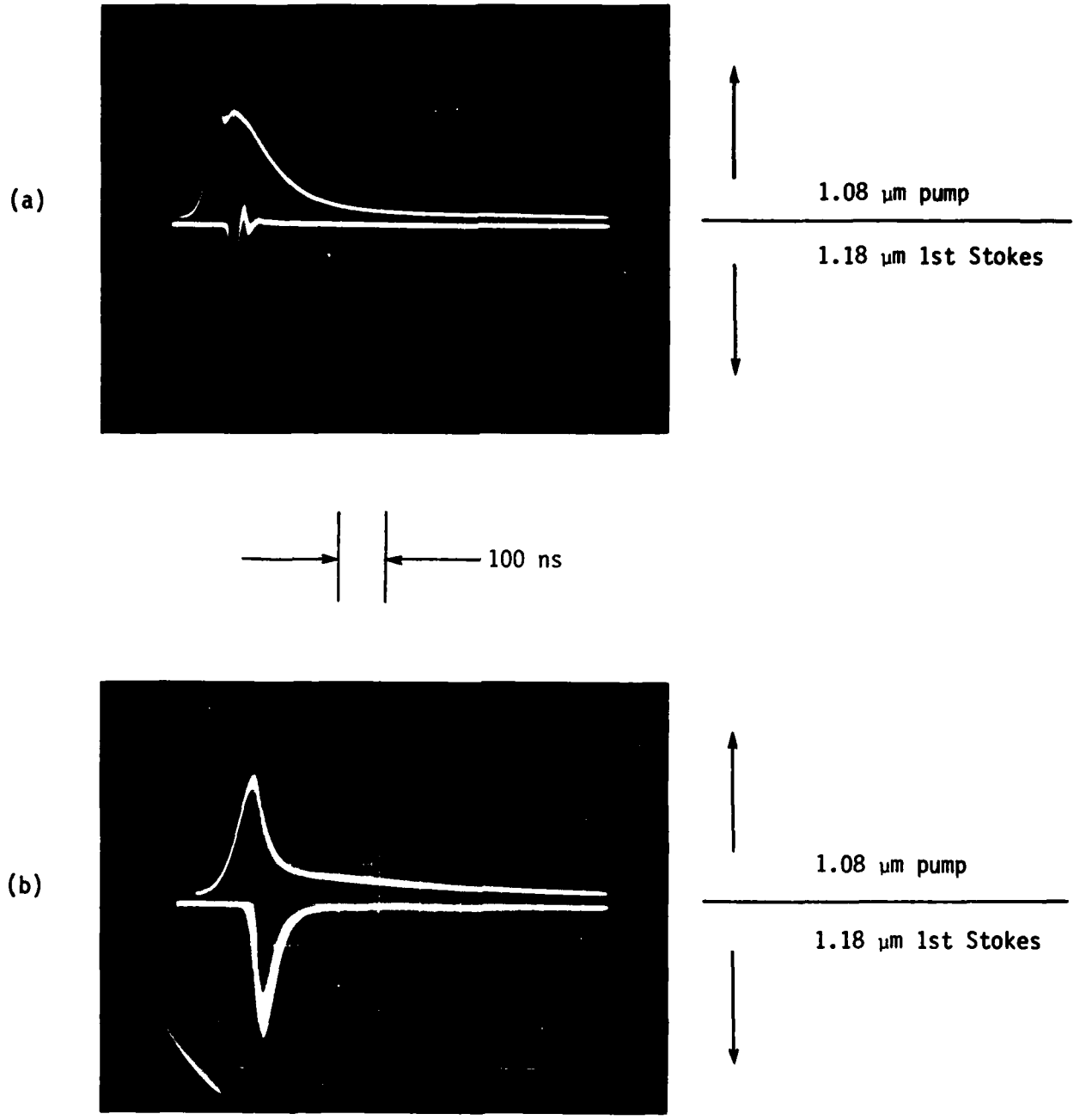

Figure 19. Pump Pulse Depletion for SRS in (a) Three-Mirror Configuration and (b) Two-Mirror Configuration

The importance of this residual 1.08μm energy is demonstrated by the results shown in Figure 20. The upper trace shows 1.08μm pump depletion when the $LiIO_3$ is rotated so that no 0.565μm SFG occurs. This depletion is due to SRS alone. When the $LiIO_3$ is rotated so that 0.565μm SFG is phase-matched, pump depletion takes the form shown in the lower trace of Figure 20. The pump pulse is now depleted to a greater depth. The initial portion of this depletion is due to SRS, but the remainder is due to 0.565μm SFG.

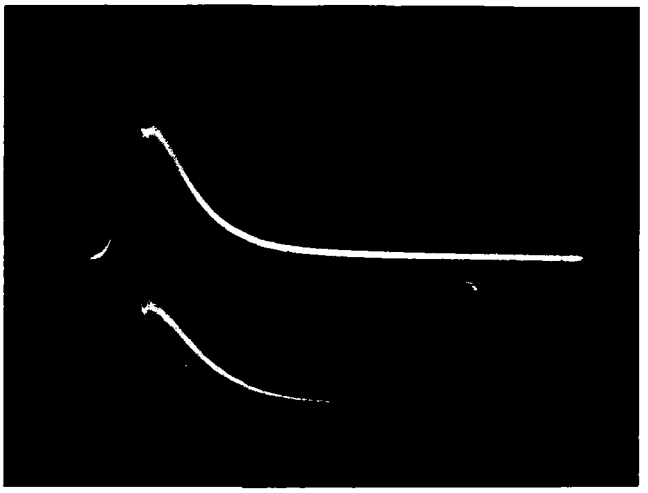

Figure 20. Pump pulse depletion for SRS alone (upper trace) and for simultaneous SRS and SFG (lower trace)

After the power-versus-PRF data of Figure 19 had been taken, we set the laser PRF at 3 kHz and carefully adjusted the $LiIO_3$ crystal and all three mirrors for maximum 0.565μm power output. This systematic adjustment procedure produced a best average output power of 218 milliwatts. Because an equal amount of "wrong-way" 0.565μm power was also being generated, we have some 400 milliwatts of recoverable 0.565μm power.

The three-mirror 0.565μm pulses were found to be about 6 nanoseconds in duration (FWHP), with the corresponding 1.18μm pulses also 6 nanoseconds long. Thus, unlike the SHG situation, we do not observe any stretching of the 1.18μm pulse in the

presence of SFG. Figure 21 shows an oscilloscope photograph of the 0.565μm pulses. It can be seen that the rise time (10 to 90 percent) and fall time are each approximately 3 to 4 nanoseconds, and that the pulse shape is reasonably symmetric. We note that the photograph of Figure 21 actually shows 750 pulses that are superimposed.

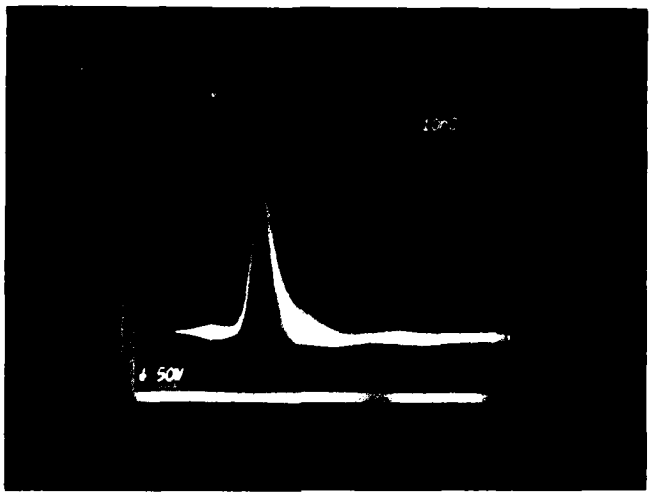

Figure 21. 0.565μm pulses obtained from three-mirror SRS/SFG experiment (each large horizontal division represents 10 nanoseconds)

The rather good 0.565μm power outputs of Figure 18 would be even better if it were not for the occurrence of a deleterious effect during SFG. Namely, the occurrence of SFG tends to suppress the longer wavelength component that produces it. That is, 0.565μm SFG tends to extinguish the 1.18μm first Stokes while 0.622μm SFG tends to extinguish the 1.31μm second Stokes. The 0.565μm output powers of Figure 18 were obtained by tilting the $LiIO_3$ crystal away slightly from perfect phase-matching, thereby reducing the suppression effect. Thus, the final angle to which the $LiIO_3$ is rotated is rather critical; it is a compromise aimed at avoiding suppression of the SRS while maintaining reasonably efficient SFG. In practice, the final $LiIO_3$ angle is arrived at experimentally by maximizing the 0.565μm power output.

In Section V of this report, further theoretical and experimental results are given concerning how the presence of SHG or SFG affects SRS.

4.3 0.622μm SUM FREQUENCY

Three-mirror experiments were also carried out on the 0.622μm SF generated from first- and second-Stokes beams. In this case, the $LiIO_3$ was rotated to its phase-matching angle of $\theta = 25.4$ degrees. The resulting SF output is plotted in Figure 22 with the available 1.31μm, 1.18μm, and 1.08μm powers.

The largest one-way 0.622μm average power measured was 29 milliwatts and was achieved at a PRF of 2 kHz. This sum frequency utilizes the 1.18μm first Stokes, which is maximum at a 3 kHz PRF, and the 1.31μm second Stokes, which is maximum at a 1 kHz PRF. From our previous SRS results [4,5], we know that three-mirror SRS falls off more quickly with increasing PRF than does two-mirror SRS. This is especially true of the second-Stokes output. This is one of the reasons why three-mirror SRS/SHG/SFG average output powers are generally less than two-mirror output powers, with the decrease being most pronounced when the second Stokes is involved.

The measured 0.622μm pulse length was 4 nanoseconds. These pulses were generated from 6-nanoseconds-long 1.18μm pulses and 5-nanoseconds-long 1.31μm pulses. No stretching of either the 1.18μm or 1.31μm pulses was observed during SFG.

4.4 0.655μm SECOND HARMONIC

The $LiIO_3$ crystal was rotated to $\theta = 24.2$ degrees and phase-matched SHG of the 1.31μm second Stokes was obtained. The resulting 0.655μm SH output together with 1.08μm and 1.31μm powers are shown in Figure 23. The largest one-way 0.655μm average power was 26 milliwatts at a 1 kHz PRF; the largest 1.31μm second-Stokes power also occurred at a 1 kHz PRF.

The three-mirror 0.655μm pulses were approximately 4 nanoseconds long and the driving 1.31μm pulses were about 5 nanoseconds long. A slight amount of 1.31μm pulse-stretching occurred here since the 1.31μm pulses were 4 nanoseconds long in the absence of SHG.

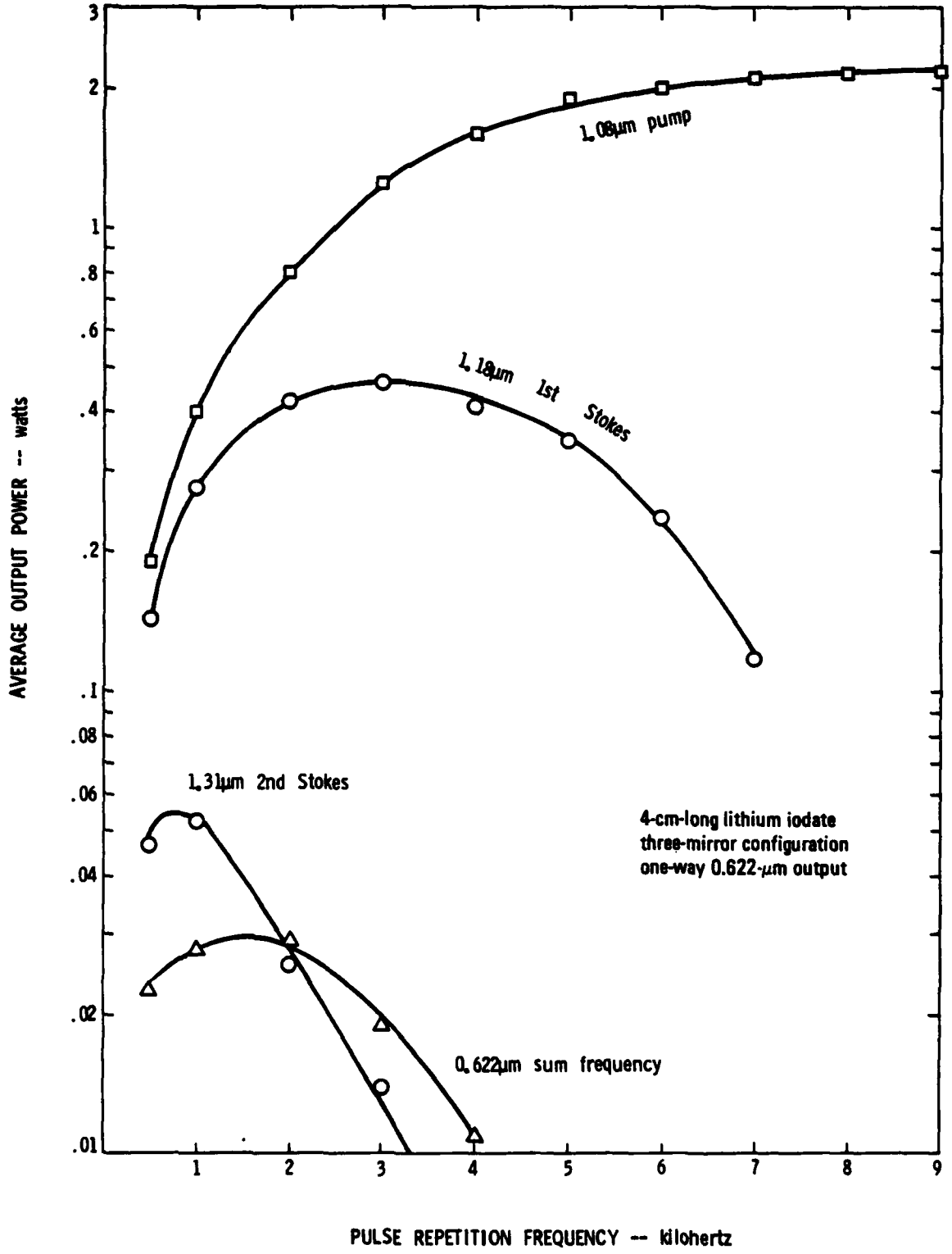

Figure 22. Pump, first-Stokes, second-Stokes, and (one-way) 0.622μm SF average powers

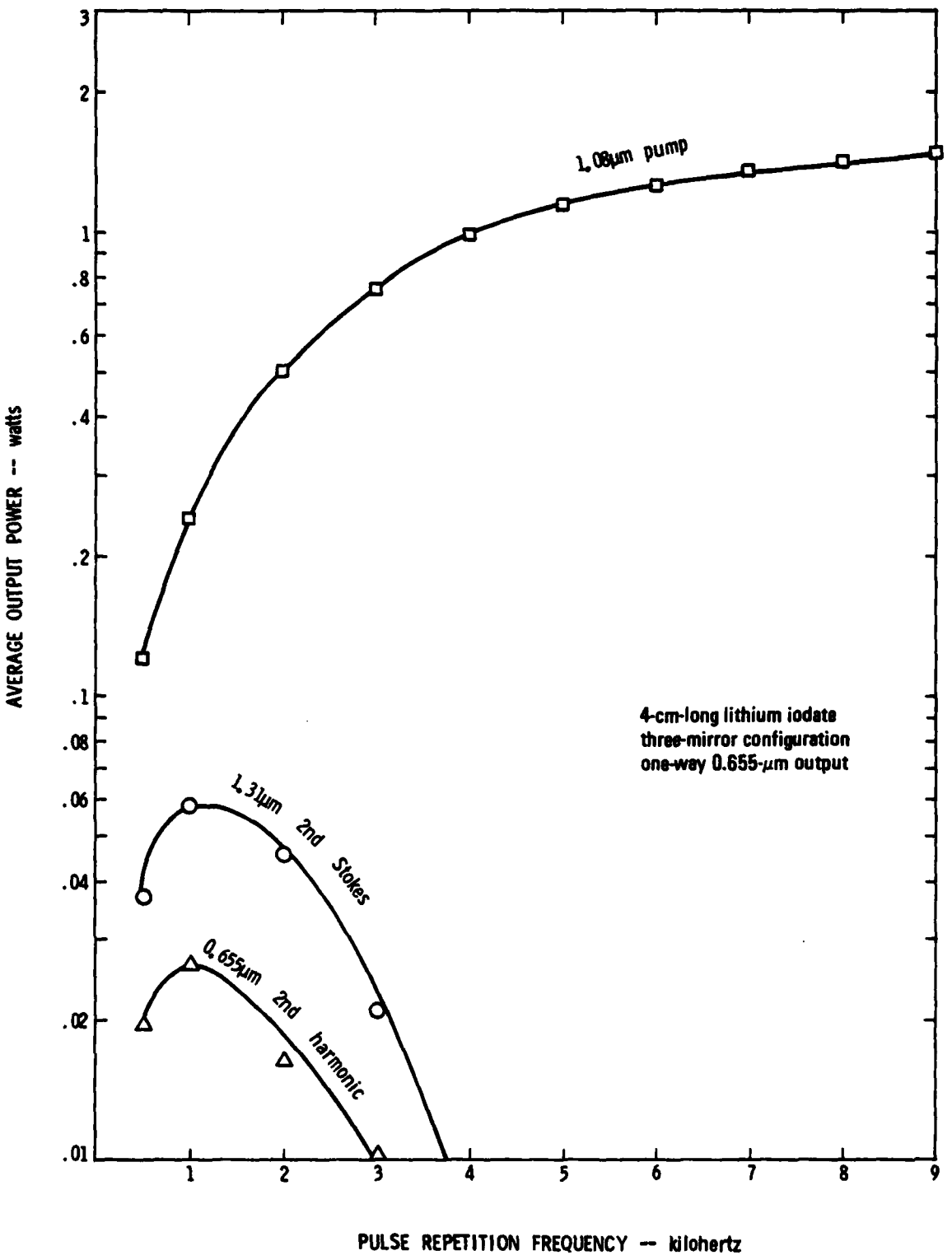

Figure 23. Pump, second-Stokes, and (one-way) 0.655μm SH average powers

4.5 0.54μm SECOND HARMONIC

The final three-mirror experiment involved conventional SHG of the 1.08μm pump. The results of this measurement are shown in Figure 24. This experiment served primarily as a general calibration of the laser, indicating the output power attainable via conventional internal SHG. From Figure 24 we see that a maximum one-way 0.54μm average power of 1.16 watts was obtained at a 5 kHz PRF. The internal mirror M_2 is actually superfluous in this experiment, because the 0.54μm SHG totally suppresses the SRS. Mirror M_2 was left in place, however, because it does contribute a certain insertion loss. By having mirror M_2 in place for all three-mirror experiments, a more meaningful comparison is possible of the five visible SH and SF outputs that are achieved.

Because SRS is not present during 0.54μm SHG, the 0.54μm pulses have the relatively long duration that is characteristic of the pumping 1.08μm pulses. In this experiment, we found the 0.54μm pulses were approximately 90 nanoseconds long.

4.6 SUMMARY OF THREE-MIRROR SRS/SHG/SFG RESULTS

The results obtained with the three-mirror configuration are summarized in Table II. For purposes of uniformity, all results listed in Table II are for a 3 kHz PRF. It should be noted, however, that the average power of several of the visible outputs is greater at some PRF other than 3 kHz. Some two-mirror SRS/SHG/SFG results are also included in Table II for purposes of comparison.

Table II. Three-mirror and two-mirror SRS/SHG/SFG powers obtained at a 3 kHz PRF.

OUTPUT WAVELENGTH	NONLINEAR PROCESS	THREE-MIRROR AVERAGE OUTPUT POWER	THREE-MIRROR PULSE LENGTH	THREE-MIRROR PEAK PULSE POWER	TWO-MIRROR AVERAGE OUTPUT POWER	TWO-MIRROR PULSE LENGTH	TWO-MIRROR PEAK PULSE POWER
0.540 μm	SHG	950 mW	90 ns	3.52 kW	1.13 W	160 ns	2.35 kW
0.565 μm	SFG	127 mW	6 ns	7.05 kW	78 mW	40 ns	.65 kW
0.592 μm	SHG	191 mW	11 ns	5.79 kW	472 mW	45 ns	3.50 kW
0.622 μm	SFG	19 mW	4 ns	1.57 kW	98 mW	30 ns	1.08 kW
0.655 μm	SHG	10 mW	4 ns	.83 kW	107 mW	25 ns	1.43 kW
1.080 μm		1.50 W	140 ns	3.56 kW	2.0 W	140 ns	4.75 kW

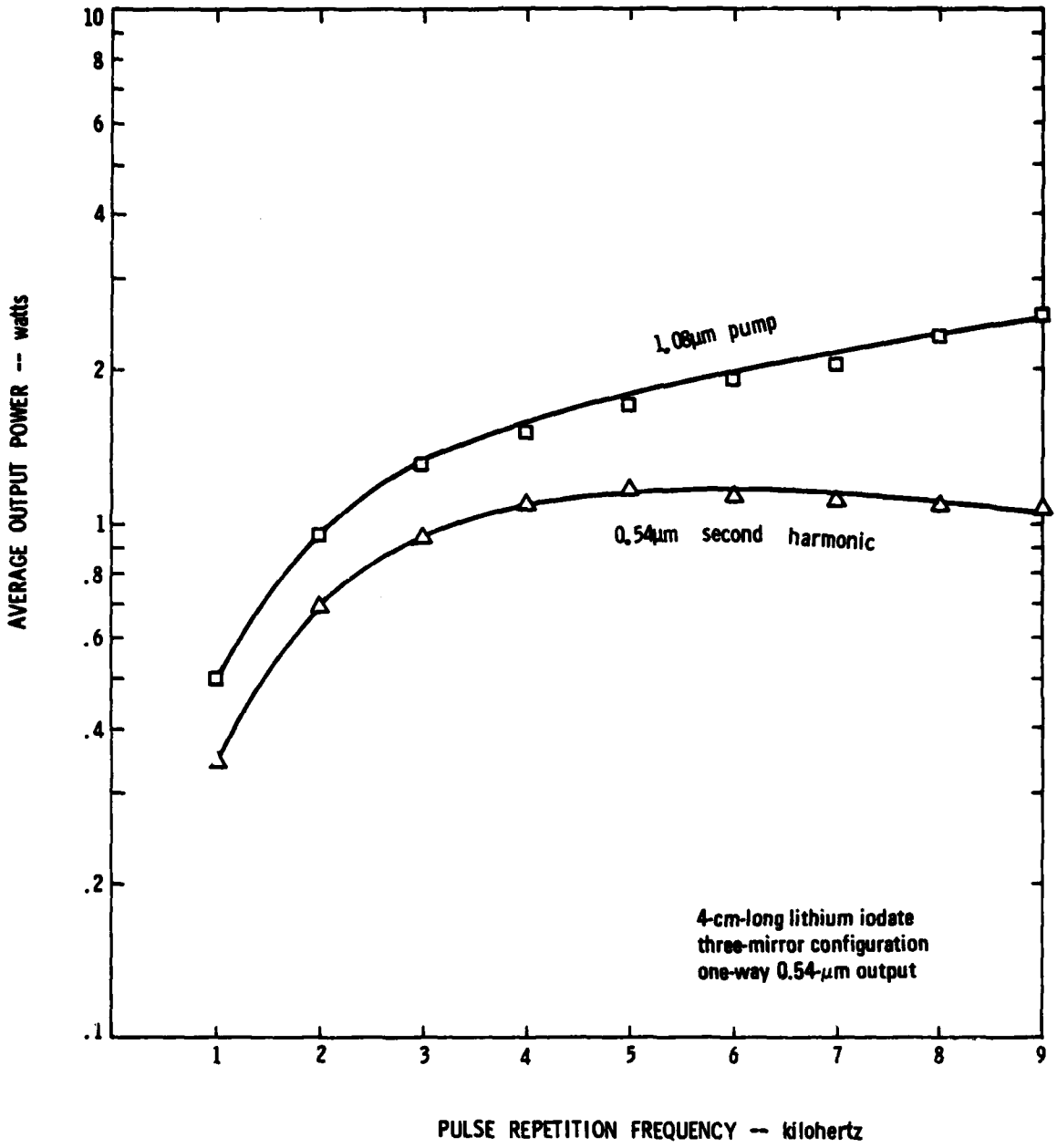

Figure 24. Pump and (one-way) 0.54μm SH average powers

We conclude that two-mirror SRS/SHG/SFG average powers are generally greater than corresponding three-mirror powers. An exception to this is the 0.565μm SF output, which is larger and more stable for the three-mirror configuration. The three-mirror configuration yields SH and SF pulses that are only a few nanoseconds in duration. As a result, peak pulse powers are typically larger for the three-mirror case than for the two-mirror case even through average powers are less.

The three-mirror and two-mirror configurations thus tend to produce SRS/SHG/SFG results that are complementary. For a given application, one can effectively trade off peak power against average power by choosing between two-mirror and three-mirror configurations.

Section V

INTERACTIONS BETWEEN SRS, SHG, AND SFG

In the SRS/SHG/SFG device, two different processes occur simultaneously when each visible output is generated. Either simultaneous SRS and SHG, or simultaneous SRS and SFG are occurring in the $LiIO_3$ crystal. These pairs of processes interact, thereby causing some interesting effects. To help understand these interactions, we have analyzed the behavior of these simultaneous processes on this program.

The basic coupled nonlinear equations have been derived for two of the main cases of interest: (1) SHG of the first-Stokes beam, and (2) SFG of the pump and first-Stokes beams. These two cases are discussed in the following paragraphs.

5.1 INTERACTIONS BETWEEN SRS AND SHG

For simultaneous SRS and SHG, the pertinent equations are:

$$\frac{dE_S}{dz} = RI_L E_S - iHE_S^* E_{SH} e^{-i\Delta kz} \tag{9}$$

$$\frac{dE_{SH}}{dz} = -iH' E_S^2 e^{i\Delta kz} \tag{10}$$

where E_S and E_{SH} are the first-Stokes and second-harmonic electric fields, respectively, I_L is the pump intensity, R contains constants pertaining to the SRS, H and H' contain constants pertaining to the SHG process, Δk is the SHG wavevector mismatch, and the asterisk denotes complex conjugate.

In deriving Equations 9 and 10, we have made the following simplifying assumptions. First we have assumed a continuous, rather than pulsed, system and have therefore set all time derivative terms equal to zero. Second, we have assumed that all components are plane waves. Third, we have assumed that no losses are present at either the first-Stokes or second-harmonic wavelengths. Finally, we have assumed that there is no pump depletion. With the assumptions we have made, it is

obvious that the equations will not predict the large signal, time varying behavior (pulses, depletion, etc.) of the SRS/SHG/SFG device. However, we are primarily interested in determining how SRS threshold is affected by the presence of SHG and SFG, and the aforementioned assumptions should be valid in this case.

If we write the compled E_S and E_{SH} quantities in terms of amplitude (ϵ) and phase ($e^{i\phi}$) terms

$$E_S = Re \left[\epsilon_S e^{i\phi_S} e^{i(k_S z - \omega_s t)} \right]$$

and $$E_{SH} = Re \left[\epsilon_{SH} e^{i\phi_{SH}} e^{i(k_{SH} z - \omega_{SH} t)} \right] ,$$

Equations (9) and (10) then become

$$\frac{d\epsilon_S}{dz} = RI_L \epsilon_S + H \epsilon_S \epsilon_{SH} \sin\theta \tag{11}$$

$$\frac{d\epsilon_{SH}}{dz} = - H' \epsilon_S^2 \sin\theta \tag{12}$$

$$\frac{d\theta}{dz} = \left[\frac{2H\epsilon_{SH}^2 - H'\epsilon_S^2}{\epsilon_{SH}} \right] \cos\theta \tag{13}$$

where $\theta = \phi_{SH} - 2\phi_S$.

Solving Equations 11, 12, and 13 simultaneously, the resulting final expression for $\epsilon_S(z)$ is

$$\varepsilon_S(z) = \frac{\varepsilon_S(0)e^{RI_L z}}{1 + \frac{HH'\varepsilon_S^4(0)}{4\left[RI_L\varepsilon_S(0)\right]^2}\left(e^{2RI_L z}\right)} \tag{14}$$

where $\varepsilon_S(0)$ is the initial amplitude of the Stokes wave as it begins to grow from noise.

The following conclusions can be drawn from the final result given in Equation 14:

a. The small-signal gain for $\varepsilon_S(z)$ can be shown to be approximately equal to RI_L, the same value which occurs for conventional SRS. Thus the presence of simultaneous SHG does not significantly increase SRS threshold.

b. The simultaneous SHG does introduce a saturation-type term in the denominator of Equation 14. Thus as $\varepsilon_S(z)$ grows to substantial levels, its behavior will deviate from that obtained with conventional SRS.

c. As a check, we note that when SHG is absent (H=H'=0), Equation 14 reduces to the standard expression for conventional SRS.

5.2 INTERACTIONS BETWEEN SRS AND SFG

For simultaneous SRS and SFG, the pertinent equations are:

$$\frac{dE_S}{dz} = RI_L E_S - iHE_L^* E_{SF} e^{-i\Delta kz} \tag{15}$$

$$\frac{dE_{SF}}{dz} = iH'E_L E_S e^{i\Delta kz} \tag{16}$$

where E_{SF} is the sum-frequency electric field and H and H' are constants pertaining to the sum-frequency generation process. We will once again write the complex E_S and E_{SF} quantities in terms of amplitude (ε) and phase ($e^{i\phi}$) terms

$$E_S = \mathrm{Re}\left[\epsilon_S e^{i\phi_S} e^{i(k_S z - \omega_S t)}\right]$$

and $$E_{SF} = \mathrm{Re}\left[\epsilon_{SF} e^{i\phi_{SH}} e^{i(k_{SF} z - \omega_{SF} t)}\right] .$$

Equations 15 and 16 then become

$$\frac{d\epsilon_S}{dz} = RI_L \epsilon_S + H\epsilon_L \epsilon_{SF} \sin\theta \tag{17}$$

$$\frac{d\epsilon_{SF}}{dz} = -H' \epsilon_L \epsilon_S \sin\theta \tag{18}$$

$$\frac{d\theta}{dz} = -\left[\frac{H'\epsilon_L \epsilon_S}{\epsilon_{SF}} + \frac{H\epsilon_L \epsilon_{SF}}{\epsilon_S} - \frac{H''\epsilon_{SF}\epsilon_S}{\epsilon_L}\right] \cos\theta \tag{19}$$

where $\theta = \phi_{SF} - \phi_S - \phi_L$.

Solving Equations 17, 18, and 19 simultaneously, we obtain the final result for the Stokes wave.

$$\epsilon_S = \epsilon_S(0) e^{\frac{RI_L + \sqrt{R^2 I_L^2 - 4HH'I_L}}{2} z} \tag{20}$$

We can draw the following conclusions from Equation 20 concerning how SFG affects SRS:

a. If the SFG process is absent (H=H'=0), the Stokes gain has the expected value of $g=RI_L$.

b. When SFG is present, the Stokes gain is reduced via the $4HH'I_L$ terms of Equation 20.

c. It is important to try to keep $R^2I^2 > 4HH'I_L$ so that g remains as large as possible, and so that it does not become complex. In our experimental situation where SFG extinguishes the SRS, it is likely that $R^2I_L^2 < 4HH'I_L$.

d. One can ensure that $R^2I_L^2 > 4HH'I_L$ by increasing the laser intensity I_L to a sufficiently high level. Thus it should be possible to circumvent the SRS suppression by pumping harder, as long as damage does not become a limiting factor.

5.3 EXPERIMENTAL RESULTS

Experiments have been performed that not only confirm the predicted results of Sections 5.1 and 5.2, but demonstrate some additional aspects of SRS/SHG/SFG interactions. These experiments were performed on both two-mirror and three-mirror versions of the device. A mirror having 14 percent transmission at 1.18μm was utilized as the right-hand mirror (mirror M_3 of Figure 1). In the experiments, the 1.18μm output power was continuously measured as the $LiIO_3$ crystal was rotated through various values of θ. The goal of these experiments was to see how the 1.18μm output power varied as θ was swept through the phase-matching angles for the various SHG and SFG processes.

The results for the two-mirror case are shown in Figure 25. We first note that at about $\theta = 28$ degrees, 0.565μm SFG completely extinguishes the SRS. This is in agreement with our previous calculated results of Section 5.2 that showed that 0.565μm SFG would significantly reduce the gain of the 1.18μm first-Stokes beam. Secondly, we note that at $\theta = 26.7$ degrees, 0.592μm SHG causes about a 25 percent dip in the first-Stokes output power. The measured output at this point consists of both 1.18μm and 0.592μm. Most of the dip which occurs is attributable to "wrong-way" 0.592μm SH output, rather than to a reduction in the intensity of the SRS. Thus, as our calcuations of Section 5.1 predict, SRS threshold is relatively unaffected by the presence of 0.592μm SHG.

The next feature of interest in Figure 25 is the increase in first-Stokes output which occurs at about $\theta = 26.5$ degrees. At this angle, the polished faces of

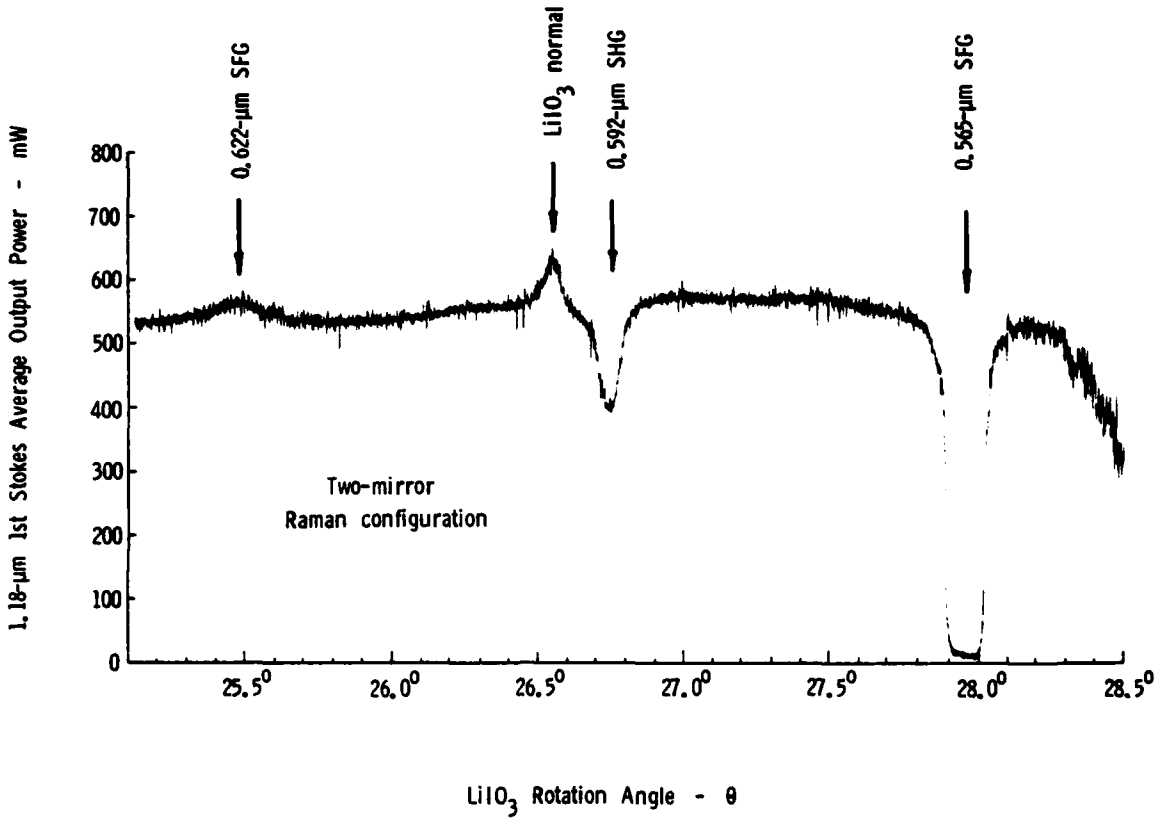

Figure 25. Effects of SHG and SFG on SRS in two-mirror Raman configuration

the $LiIO_3$ crystal are exactly normal to the 1.08μm pump beam. At normal incidence, residual 1.08μm and 1.18μm reflections from the $LiIO_3$ surfaces remain in their respective cavities, rather than being reflected out and therefore lost.

The final interesting feature of Figure 25 occurs at $\theta = 25.5$ degrees where a slight increase in 1.18μm power is seen. At this angle, SFG involving the first- and second-Stokes beams is occurring. In this case, the SFG acts to suppress the second Stokes, but not the first Stokes. Because the second Stokes is, in reality, a loss for the first Stokes, when the second Stokes is suppressed the first-Stokes output will increase. Figure 25 shows that this does occur.

A similar experiment was performed using the three-mirror configuration and the results are shown in Figure 26. The general behavior of the SRS is seen to be the same as in Figure 25. However, one additional feature emerges from the three-mirror results. The dip which occurs due to 0.565μm SFG is seen to be asymmetric. The SRS resume more quickly on the right-hand side (larger values of θ) of the dip than it does on the left-hand side, and reaches a larger value. Thus, the right-hand side should be the preferred location when generating the 0.565μm SF. This postulate was confirmed by a three-mirror 0.565μm experiment. Using the "right-hand shoulder" of the dip, a 3 kHz output power of 218 milliwatts was obtained. Using the left-hand shoulder of the dip, a 3 kHz power of only 40 milliwatts was obtained. We note that 218 milliwatts represents the best 0.565μm average power we have yet achieved.

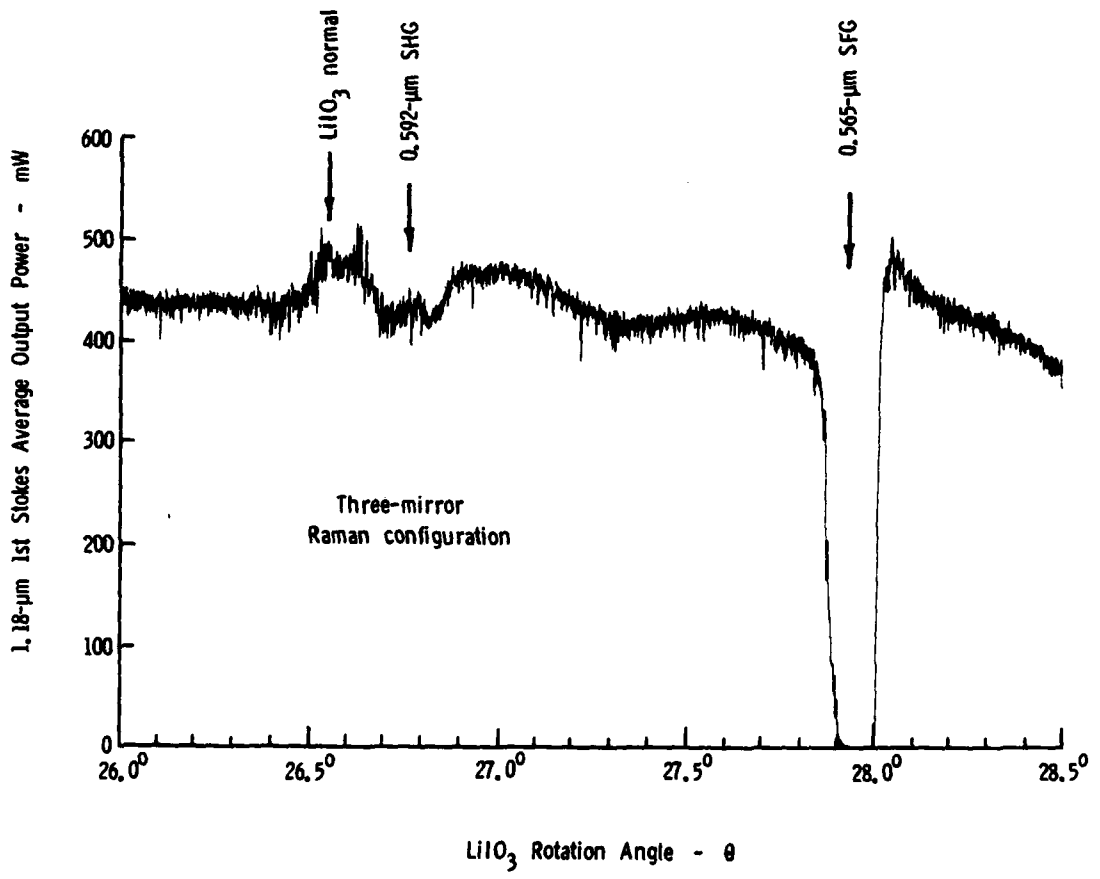

Figure 26. Effects of SHG and SFG on SRS in three-mirror Raman configuration

5.4 SUMMARY OF SRS/SHG/SFG INTERACTION EFFECTS

The following interactions have been seen to occur in the SRS/SHG/SFG device both with two-mirror and three-mirror configurations:

a. When the SH of the pump beam is generated, SRS is completely suppressed.

b. When the SF of the pump and first Stokes beams is generated, the first Stokes beam tends to be suppressed. SRS can be reinitiated by tilting the $LiIO_3$ crystal slightly so that SFG is no longer perfectly phasematched.

c. When the SH of the first Stokes beam is generated, there is relatively little effect upon the first Stokes beam. However the second Stokes beam is suppressed.

d. When the SF of the first and second Stokes beams is generated, the second Stokes beam tends to be suppressed.

e. When the SH of the second Stokes beam is generated, there is relatively little effect upon either the first or second Stokes beams.

Section VI

MISCELLANEOUS SRS/SHG/SFG RESULTS

6.1 POTENTIALLY LIMITING PROCESSES

The 0.59μm SHG experiments of Section 3.2 in which a 6-centimeter long $LiIO_3$ crystal was employed represent the highest power experiments that were carried out on this program. During the time that the data of Figure 13 was taken, we made a plot of the output spectrum of the SRS/SHG/SFG device in the near infrared. The resulting plot is shown in Figure 27.

The only spectral lines that appear in Figure 27 are the pump, first Stokes, and second Stokes beams. The absence of any other lines indicates that competing processes are not yet interfacting. In particular, no other vibrational modes in the $LiIO_3$ are producing SRS. Additionally, the narrowness of the spectral lines of Figure 27 indicates that stimulated Brillouin scattering (SBS) is not occurring. Thus we see that two of the potential competing processes have not appeared at the highest power levels at which we have operated.

We note also that damage effects are relatively minor thus far. We have seen no damage on mirrors M_1, M_2, and M_3, and have seen no surface damage on the $LiIO_3$ crystal. We have seen a slight amount of bulk damage within the 4-centimeter long $LiIO_3$ crystal, but it is limited in extent and can easily be avoided by translating the crystal.

6.2 SRS PUMPED BY VISIBLE BEAMS

Another concern has been whether one of the strong visible beams (such as 0.59μm) would act as the pump for SRS thereby producing several visible outputs simultaneously. In all our experiments to date, we have seen no evidence of this occurring. A likely reason why SH-pumped (or SF-pumped) SRS does not occur is that none of the mirrors are HR in the visible where the Stokes beams would lie. Thus there is no resonator for these Stokes beams, and they do not have sufficient gain to reach threshold during a single pass.

In summary then, we have so far not encountered any processes which compete with or limit the 818 cm^{-1} SRS that forms the basis for the SRS/SHG/SFG device.

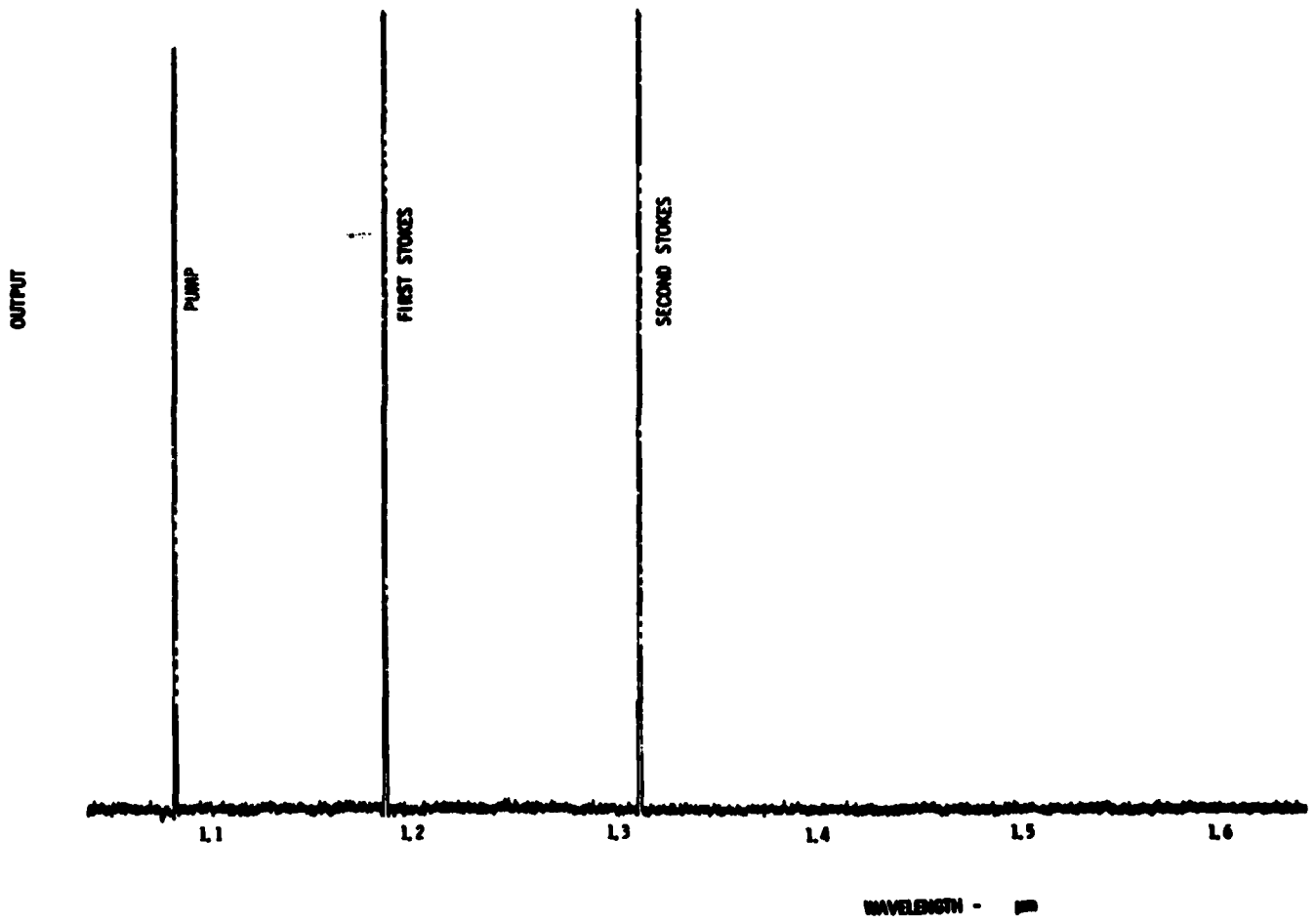

Figure 27. Output spectrum of SRS/SHG/SFG device during high power 0.592 μm generation

Section VII

SUMMARY AND CONCLUSIONS

The general goal of this program has been to study the simultaneous occurrence of stimulated Raman scattering (SRS), second harmonic generation (SHG), and sum-frequency generation (SFG) in lithium iodate. The simultaneous occurrence of these processes results in selectable, multiple outputs spanning the 0.54 to 0.65-μm portion of the visible spectrum. On this program we have found that both the SRS and the SHG or (SFG) can be very efficient in lithium iodate, yielding appreciable average and peak output powers. Thus the SRS/SHG/SFG device is interesting from a practical viewpoint as well as from a scientific viewpoint.

The SRS/SHG/SFG device that we have studied consists of a lithium iodate crystal placed inside a Nd:$YA\ell O_3$ laser. The Nd:$YA\ell O_3$ laser is continuously pumped and repetitively Q-switched at pulse repetition rates of 1 to 9 kHz. Both two-mirror and three-mirror Raman configurations were employed in this work. In the two-mirror case, the Stokes lines and the Nd:$YA\ell O_3$ laser share the same resonator; in the three-mirror case, an additional mirror is inserted within the Nd:$YA\ell O_3$ laser to form a short Stokes cavity.

Extensive SRS/SHG/SFG experiments were performed using the two-mirror Raman configuration. From this configuration, we obtained second-harmonic outputs at 0.54 μm (1.13 W), 0.592μm (685 mW), and 0.655μm (107 mW) and sum-frequency outputs at 0.565μm (78 mW) and 0.622μm (98 mW). The output pulse lengths ranged from 25 nanoseconds to 40 nanoseconds giving peak pulse powers of about 1 to 4 kW.

SRS/SHG/SFG experiments were also performed using the three-mirror configuration. In the three-mirror case, the outputs were 0.54μm (950 mW), 0.565μm (218 mW), 0.592μm (202 mW), 0.622μm (29 mW), and 0.655μm (26 mW). The SH and SF average powers are generally less in the three-mirror case than the two-mirror case because the Stokes powers are generally lower. However the three-mirror SH and SF pulses are very short, being typically 4 to 10 nanoseconds long. As a result, the peak powers are typically larger for the three-mirror case than for the two-mirror case even though average powers are less.

In the SRS/SHG/SFG device, two different processes occur simultaneously when each visible output is generated. Either simultaneous SRS and SHG, or simultaneous SRS and SFG are occurring in the lithium iodate crystal. These pairs of processes interact, thereby causing some interesting effects. We have analytically and experimentally studied these interactions on this program. Our results are that for simultaneous SRS and SHG, the presence of the SHG does not significantly increase SRS threshold. On the other hand, when simultaneous SRS and SFG occurs the SFG significantly increases threshold for the SRS process. In fact, when the lithium iodate is rotated for perfect SFG phasematching, the SRS is completely suppressed in our experiments. The SF outputs obtained in this work are achieved by rotating the lithium iodate slightly away from perfect SFG phasematching, thereby reducing the suppression effect.

The SRS/SHG/SFG laser studied on this program is appealing from a practical standpoint for a number of reasons:

a. The device is entirely solid-state.

b. The tuning from line to line is accomplished by means of a single adjustment (crystal rotation).

c. The device is very simple, consisting in the two-mirror case of only an AR-coated lithium crystal placed inside a Nd:$YA\ell O_3$ laser.

d. There are no thermal effects to combat in the lithium iodate. Both the SRS and the SHG/SFG processes in lithium iodate are essentially temperature independent.

Finally we note that it should be possible to increase the average output power of the SRS/SHG/SFG device into the watt region by utilizing Nd:YAG as the pump laser instead of Nd:$YA\ell O_3$, and by further studies aimed at optimizing the Raman cavity and Raman medium that are utilized. In addition it should also be possible to extend the SRS/SHG/SFG outputs into the more covert 0.65μm to 0.85μm region either by utilizing the third and fourth Stokes outputs for SHG and SFG, or by pumping SRS/SHG/SFG with the 1.32μm output of Nd:YAG.

Section VIII

PUBLICATIONS

The following articles have been (or will be) submitted to technical journals for publication. Support from this contract was acknowledged in each instance.

1. E. O. Ammann, "Simultaneous Stimulated Raman Scattering and Optical Frequency Mixing in Lithium Iodate," Appl. Phys. Lett., vol. 34, pp. 838-840, 15 June 1979.
2. E. O. Ammann, "Simultaneous Stimulated Raman Scattering and Optical Frequency Mixing Employing a Three-Mirror Configuration," (to be submitted to J. Appl. Phys.)
3. E. O. Ammann, "Interactions between Simultaneously Occurring Stimulated Raman Scattering, Second Harmonic Generation, and Sum Frequency Generation," (to be submitted to J. Appl. Phys.)

This Page Left Intentionally Blank

Section IX

REFERENCES

1. E.O. Ammann, "Lithium Iodate Parametric Oscillator," final report on WPAFB Contract No. F33615-74-C-1014, June 1975.

2. E.O. Ammann, "Stimulated Raman Scattering at kHz Pulse Repetition Rates," final report on ERDA Contract No. E(04-3)-1245, May 1977.

3. E.O. Ammann and J. Falk, "Stimulated Raman Scattering at kHz Pulse Repetition Rates," Appl. Phys. Lett., vol. 27, pp. 662-664, 15 December 1975.

4. E.O. Ammann and C.D. Decker, "0.9-W Raman Oscillator," J. Appl. Phys., vol. 48, pp. 1973-1975, May 1977.

5. E.O. Ammann, "High-Average-Power Raman Oscillator Employing a Shared-Resonator Configuration," Appl. Phys. Lett., vol. 32, pp. 52-54, 1 January 1978.

6. W.S. Otaguro, E. Wiener-Avnear, and S.P.S. Porto, "Determination of the Second-Harmonic-Generation Coefficient and the Linear Electro-Optic Coefficient in $LiIO_3$ through Oblique Raman Phonon Measurements," Appl. Phys. Lett., vol. 18, 1 June 1971, pp. 499-501.

7. W. Otaguro, E. Wiener-Avnear, C.A. Arguello, and S.P.S. Porto, "Phonons, Polaritons, and Oblique Phonons in $LiIO_3$ by Raman Scattering and Infrared Reflection, Phys. Rev. B, vol. 4, pp. 4542-4551, 15 December 1971.

8. W. Otaguro, C.A. Arguello, and S.P.S. Porto, "Mixing of Internal Modes of Different Molecular Symmetry in $LiIO_3$," Phys. Rev. B, vol. 1, pp. 2818-2820, 15 March 1970.

9. W.S. Otaguro, E. Wiener-Avnear, S.P.S. Porto, and J. Smit, "Oblique Polaritons in Uniaxial Crystals: Application to $LiIO_3$," Phys. Rev. B, vol. 6, pp. 3100-3104, 15 October 1972.

10. A.J. Campillo, "Properties of a Pulsed $LiIO_3$ Doubly-Resonant Parametric Oscillator," IEEE J. Quant. Electron., vol. QE-8, pp. 809-811, October 1972.

11. E.O. Ammann, "Simultaneous Stimulated Raman Scattering and Optical Frequency Mixing in Lithium Iodate," Appl. Phys. Lett., vol. 34, pp. 838-840, 15 June 1979.

12. E.O. Ammann, "Simultaneous Stimulated Raman Scattering and Optical Frequency Mixing Employing a Three-Mirror Raman Configuration," (to be submitted to J. Appl. Phys.)

13. J.E. Murray and S.E. Harris, "Pulse Lengthening Via Overcoupled Internal Second-Harmonic Generation," J. Appl. Phys., vol. 41, pp. 609-613, February 1970.

14. J.F. Young, J.E. Murray, R.B. Miles, and S.E. Harris, "Q-Switched Laser with Controllable Pulse Length," Appl. Phys. Lett., vol. 18, pp. 129-130, 15 February 1971.